Høgskulen på Vestlandet

MASTER'S THESIS

Modeling of flood and retention in the Sogn allotment garden

Atefeh Kari Jafari

Climate Change Management

Department of Environmental Sciences

Supervisor (Thorben Dunse)

07.06.2022

Western Norway University of Applied Sciences

Modeling of flood and retention in the Sogn allotment garden

Master thesis in Climate Change Management

Author: Atefeh Kari Jafari	Author sign. Atefeh Kari Jafari

Thesis submitted: Spring 2022	Open thesis

Main Supervisor: Thorben Dunse

Co-supervisors: Ashenafi Seifu Gragne (NIVA), Line Johanne Barkved (NIVA)

Keywords: Runoff, SWMM modeling, infiltration, allotment garden, inundation, peak discharge, flood extent	Number of pages: 64 + Appendix: 6 Sogndal, 07.06.2022

This thesis is a part of the master's program in Climate Change Management (Planlegging for klimaendringer) at the Department of Environmental Sciences, Faculty of Engineering and Science at the Western Norway University of Applied Sciences. The author(s) is responsible for the methods used, the results that are presented and the conclusions in the thesis.

Western Norway University of Applied Sciences

Preface

This master's thesis was carried out as the final part of the two-year master's program in Climate Change Management at Western Norway University of Applied Sciences. The research was completed in one semester, Spring 2022, and has a credit value of 30ECTS.

I am very thankful to my supervisors, Thorben Dunse, Ashenafi Seifu Gragne (NIVA), and Line Johanne Barkved (NIVA), for their guidance, help, and support. I am also grateful to Norwegian Institute for Water Research (NIVA) for proposing this research project and providing this opportunity for me to gain knowledge in flood modeling.

I would like to thank Kamilla Hauknes Sjursen, my teacher in the runoff management course, for her help and encouragement. In addition, thanks to all the other teachers at HVL and friends that helped me during the project.

I would also like to especially thank my husband, who encouraged me during those hard and stressful days and provided me with a good environment and moral support. I have saved thanks to my lovely parents and brothers, who were always beside me and encouraged me to fulfill my education in climate change management.

Western Norway University of Applied Sciences

Abstract

More frequent and severe rainfall due to climate change, on the one hand, and more impervious surfaces due to urbanization, on the other hand, are increasing the risk of urban floods. Sogn allotment garden is mainly a green area located in an urban region in Oslo that offers natural retention. However, due to the terrain and soil condition and the surrounding area's characteristics, the allotment garden is also vulnerable to stormwater inundation. This study aims to model stormwater in the Sogn allotment garden and its adjacent regions that contribute to flood inundation in the area and estimate the inundation by source (within the garden vs. adjoining areas). It also aims to map the extent of the inundation.

The hydrological analysis and flood modeling were carried out through Geographic information system (GIS) and Storm Water Management Model (SWMM). GIS was utilized for streamlines generation and subcatchment delineation and to produce parameters such as slope and width of subcatchments as input data for the SWMM model. In addition to the GIS outputs, meteorological and site boundary condition data were employed as input data in the SWMM model. The model was run based on continuous simulation for the period of 01.01.2017 to 25.02.2022.

The model simulation results provided time series of runoff, infiltration, and evaporation. The model also estimated peak runoff events and maximum water depth, which was further used to generate flood inundation maps in GIS. Based on the volume and peak of the runoff from subcatchments generated by the model and further calculations on them, the sources of stormwater runoff were identified.

The results revealed that the main source of runoff in the study area is outside the allotment garden, from where runoff flows towards the garden. The garden, due to its terrain condition and the presence of the depression, encompasses larger inundated areas than outside the garden. However, the source of the runoff leading to inundation is mainly the adjacent areas outside the garden due to more impervious land cover and hence less infiltration than the allotment garden.

Western Norway University of Applied Sciences

Sammendrag på norsk

Hyppigere og kraftigere nedbør på grunn av klimaendringer, og mer ugjennomtrengelige overflater på grunn av urbanisering, øker risikoen for urban flom. Sogn kolonihage er i hovedsak et grøntområde som ligger i en byregion i Oslo som tilbyr naturlig bevaring. På grunn av terrenget, jordsmonnet og egenskapene til det omringede området er hagen også sårbar for oversvømmelse. Denne studien tar sikte på å modellere overflatevann i Sogn kolonihage og dens tilstøtende regioner som bidrar til flomoversvømmelse i området og å estimere oversvømmelsen etter kilde (innenfor hagen vs. tilstøtende områder). Den tar også sikte på å kartlegge omfanget av oversvømmelsen.

Den hydrologiske analysen og modelleringen ble utført gjennom Geografisk informasjonssystem (GIS) og Storm Water Management Model (SWMM). GIS ble brukt for å effektivisere generering og avgrensning av delområde, samt å produsere parametere som helning og bredde på delområder som inndata for SWMM-modellen. Utdataene fra GIS samt meteorologiske data ble brukt som inndata i SWMM-modellen. Modellen ble kjørt basert på kontinuerlig simulering for perioden 01.01.2017 til 25.02.2022.

Resultatene av modellsimuleringen ga en tidsserie med avrenning, infiltrasjon og fordampning. Modellen estimerte også toppavrenningshendelser og maksimal vanndybde som videre ble brukt til å generere flomoversvømmelseskart i GIS. Basert på volumet og toppen av avrenningen fra delområder generert av modellen og videre beregning på disse ble kilden til overvannsavrenning identifisert.

Resultatene viste at hovedkilden til overflatevann i studieområdet er fra utsiden av kolonihagen som renner inn mot hagen. Hagen omfatter -på grunn av terrengtilstanden og tilstedeværelsen av forsenkningen- større oversvømmede områder enn utenfor hagen. Kilden til avrenningen som fører til oversvømmelse er imidlertid hovedsakelig tilstøtende områder utenfor hagen på grunn av mer ugjennomtrengelig arealdekke og dermed mindre infiltrasjon enn parsellhagen.

Western Norway University of Applied Sciences

Table of contents

Western Norway University of Applied Sciences

List if figures

Western Norway University of Applied Sciences

List of Tables

1 Introduction

Flooding is becoming more likely due to climate change which increases the severity and frequency of rainfalls (Jamali et al., 2018; Wilby & Keenan, 2012). Urban areas with anthropogenic changes in land covers altering hydrological processes are particularly vulnerable to flooding (Guo et al., 2021). Urbanization makes the surfaces impermeable and causes a loss of infiltration and thus a decrease in water stored in the ground (Li et al., 2020). As a result, a significant portion of stormwater volume passes over the land surfaces, increasing the risk of flooding in urban areas (Feng et al., 2021).

Urban flooding causes direct damage to property and critical infrastructure (such as energy substations and roadways) and indirect damage such as losses from utility outages, supply chain disruptions, and lost productivity (Guo et al., 2021). Surface runoff can also carry pollutants over impervious surfaces, leading to the deterioration of surface water quality (Müller et al., 2020). Therefore, studying urban floods, their causes, and their impacts is critical when considering sustainable water management, cities' future, and resilience to climate change (Serre & Heinzlef, 2018).

Effective surface water management is mainly about managing surface water locally, with a strategy that allows water to infiltrate, be stored, delayed, and purified locally as much as possible (NIVA, 2018). Conventional flood mitigation measures rely heavily on engineered structures. These structural measures are effective but not sustainable because the flood risk is transferred downstream, and they are costly and time-demanding (Huang et al., 2020).

Therefore more sustainable measures and, at the same time, economical, easy to maintain, and not requiring intensive construction have gained more attention in cities (Green et al., 2021). Cities are increasingly focusing on moving from mainly conventional water management, where the water is handled in pipes, to nature-based water management, where the water is handled in the open (NIVA, 2018). The nature-based measures can regulate runoff quantity, manage runoff quality, and provide amenities and biodiversity in a natural way (Lamond & Everett, 2019).

Oslo Municipality has a surface water strategy for 2013-2030, where the intention is to get rid of surface water that creates problems and use this water as a resource in the urban environment (NIVA, 2018). The strategy has been followed up with an action plan so that both new and existing areas are developed in a more sustainable and climate-adapted direction. The action plan defines five prioritized topics, including developing model projects (NIVA, 2018).

Flood models are robust simulation tools to examine the complexity of hydrological responses of a catchment to precipitation events and assess flood dynamics, distribution, and extent of flood inundation (Qi et al., 2021; Singh et al., 2021). The models build on detailed hydraulic and hydrological data to simulate the physical process of urban flooding (Qi et al., 2021). The outcome of the models is helpful information in mitigating floods, coming up with the most cost-effective solution, and minimizing its consequences (Bulti & Abebe, 2020). Currently, MIKE 21, InfoWorks-ICM SCS, HydroCAD, SCALGO Live, and Storm Water Management Model (SWMM), are some examples of commonly used flood simulation software for researching urban runoff (Li et al., 2018).

This study focuses on modelling stormwater runoff using EPA SWMM and estimating flood generation by source in the Sogn allotment garden and its nearby regions in the lower parts of the Gaustad catchment in Oslo. The Sogn allotment garden is a green area that provides natural retention in an urban setting. However, the site and spots inside the allotment garden are vulnerable to stormwater inundation. This research aims to examine the flood dynamic and shed light on the potential role of the allotment garden in flood retention in the area.

1.1 Objectives of the study

- Quantifying the stormwater runoff into Sogn allotment garden and evaluating contribution to inundation by sources (generated within the garden vs. runoff from adjoining areas).
- Mapping the extent of the inundation locations.

2 Theoretical framework and background

2.1 Water balance

The entering and exiting water in a catchment are defined by the hydrologic water balance. The entering water is precipitation that evaporates further, infiltrates into the soil, or runs off into rivers and lakes as surface runoff (Storteig, 2019). The penetrated water might be kept as groundwater in the soil. When rivers and lakes are lower than the groundwater table, groundwater flow moves towards them. Depending on water input, the groundwater flux varies with the seasons (Dingman, 2015, p. 389). Water vapor lost from the catchment is referred to as evapotranspiration. The process of evapotranspiration includes evaporation from the land surface and bodies of water and transpiration from vegetation (Dingman, 2015, pp. 18,71,253). The volume of the components in the water cycle over a given time interval is described by the water budget equation (equation 2.1) (Bjørvik, 2021; Welty, 2009)

$$\text{Precipitation} = \text{Runoff} + \text{Evapotranspiration} + \text{Net Groundwater outflow} + \Delta\text{Storage} \qquad (2.1)$$

The natural water cycle is disturbed in urban areas (figure 2-1), where permeable surfaces such as vegetated areas have been largely replaced with impermeable ones such as buildings, roadways, and parking lots (Moheseen, 2015).

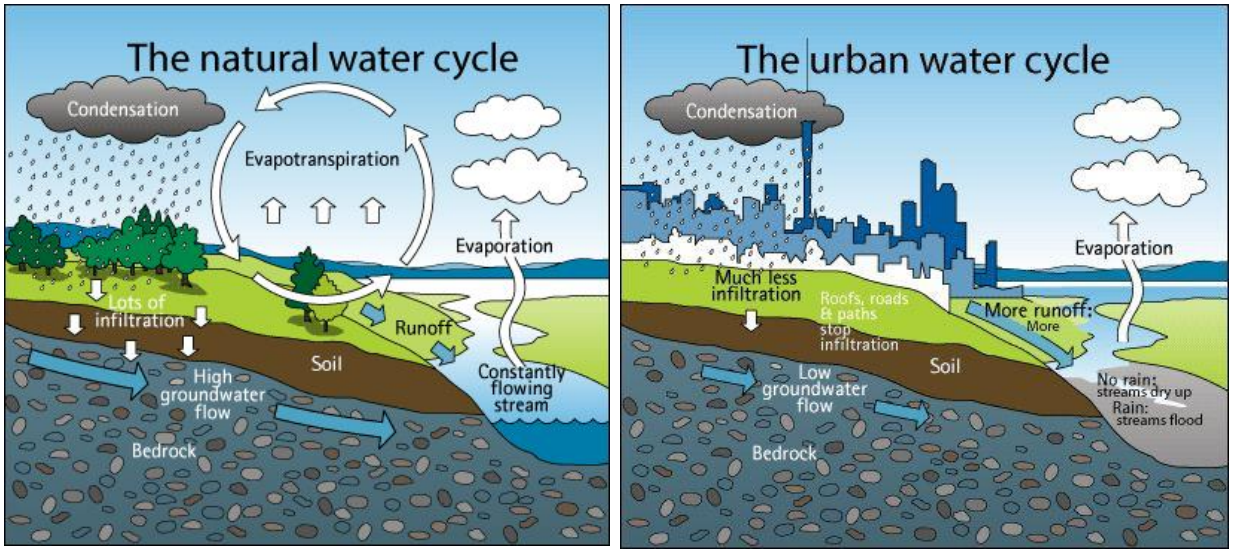

Figure 2-1: Illustration of the hydrologic cycle with the water pathways and the comparison between natural (left) and urban (right) catchments. The figure is from nationalgeographic.org.

The components in the water balance and the urbanization impacts on them are described below.

2.1.1 Precipitation and evapotranspiration

Precipitation depending on the air temperature, can happen in the form of rain or snow (Dingman, 2015, p. 133). Part of the precipitation can be caught and stored by the canopies and vegetation temporarily, known as interception. Intercepted water can later evaporate, infiltrate, or contribute to the surface flow. The magnitude of interception in urban areas is less than 1 mm, and it is either ignored or accounted for as part of the depression storage (Storteig, 2019). The occurrence, intensity, and pattern of rain might be affected by urbanization due to higher temperatures and changes in wind patterns in urban areas (Storteig, 2019).

Evaporation is when water vaporizes into the atmosphere due to temperature and solar radiation. The water vapor can then be moved to landmasses by wind systems, where it falls as precipitation (Storteig, 2019). Evaporation is one of the most significant contributors to soil-vegetation-atmosphere water and energy redistribution (Velpuri et al., 2013). Compared to natural areas, urban areas have significantly lower evaporation due to the loss of vegetation and natural water storage (Dupont et al., 2006). Evaporation decreases from almost 55 percent in natural areas to approximately 4 percent in urbanized areas for a storage capacity of 0.25-0.5 mm for urban surfaces such as roads and buildings (Bjørvik, 2021).

2.1.2 Infiltration, runoff, and groundwater

Infiltration is the vertical movement of water from rainfall or snowmelt from the ground surface into the soil. The water infiltrated into the upper unsaturated zone of the soil can later evaporate or percolates into the groundwater. The rate of infiltration is determined by the material's permeability, rainfall or snowmelt intensity, soil condition previous to the rainfall, and modifications by humans on the ground surface and subsurface (Dingman, 2015, pp. 345-355;358). In urban areas, the result of replacing pervious regions with impermeable areas is a decrease in infiltration and an increase in surface runoff (Fletcher et al., 2015).

Surface runoff is the process of flowing water on the surface due to a higher precipitation rate than infiltration rate (Bjørvik, 2021). The lower infiltration rate than precipitation is attributed to more impermeable surfaces or soil saturation. Saturation mainly happens due to the low conductivity of the soil (Storteig, 2019). It may also occur if the water table rises to the surface, usually as a result of a high groundwater level (Dingman, 2015, p. 483). The water not contributing to the runoff infiltrates into the ground.

After the water infiltrates into the unsaturated zone, the water can percolate to the saturated zone (Dingman, 2015, p. 345). The groundwater flow takes place in the saturated zone, based on the principles of Darcy's law. Groundwater aquifers act as a reservoir for water and prolong the water cycle (Bjørvik, 2021). The distribution of rain after hitting the ground changes as impervious surfaces increase, from partial to complete surface runoff (Shuster et al., 2005). As a result, the groundwater recharge may decrease. On the other hand, the groundwater recharge could increase due to the leakage from the drinking water network (Storteig, 2019).

2.2 Climate change, urbanization, and urban flooding

Rapid urbanization, combined with climate change, has resulted in many inseparable challenges (Alexander et al., 2019). Extreme storm intensity and frequency are expected to increase as global temperature rises due to climate change (Wilby & Keenan, 2012; Zahmatkesh et al., 2015). Over the last 100 years, Norway's yearly mean temperature has risen by around 1°C, resulting in higher winter and spring stream flow, earlier snowmelt, and spring and autumn flooding. Likewise, annual precipitation has increased by 18% since 1900, with most of the increase coming after 1980 (The Norwegian Centre for Climate Services (NCCS), 2017, pp. 15, 20). By the year 2100, average annual precipitation is expected to rise by 8% and 18%, respectively, under medium and high scenarios of climate forecasts. Seasonally, the highest increase of 23% in precipitation will be in the spring, and the lowest increase of 10% will be in the summer by the end of the century (The Norwegian Centre for Climate Services (NCCS), 2017, p. 20). Consequently, flood events have been predicted to increase, especially in early spring, late autumn, and winter (Moheseen, 2015).

Similarly, fast urbanization reduces soil infiltration capacity and groundwater recharge by increasing impermeable surfaces such as pavements, roads, and roofs in urban areas. As a

result, most water goes through the land surface, increasing the risk of flooding in urban areas (Zhang et al., 2017). In Norway, cities, and towns account for 82 percent of the population, with more than one million people residing in the Oslo urban settlement (Li et al., 2020). The population of Oslo municipality is predicted to grow by 40% by 2040 (Moheseen, 2015). This expanding population demands the growth of denser urban areas, putting pressure on the urban setting and its stormwater drainage system (Wihlborg et al., 2019).

As a result of the above discussion, research about the flooding process and its mitigation measures is becoming increasingly crucial in climate change adaptation (Adhikari, 2020) and urban planning.

2.3 Flood modeling

Research into flood features such as flood-upstream and downstream, stormwater volume, and flood depth is essential for lowering urban flooding risk. The capability to calculate hydrological flows with sufficient geographical detail is essential for studying flood processes (Singh et al., 2021). Computationally based hydrological and hydraulic models have been developed since the 1970s to represent complicated urban hydrological processes in a similar but simpler structure (Singh et al., 2021).

Hydrological and hydraulic models are now widely recognized as vital tools for managing excess water. Hydraulic models have typically been used to simulate the flow across river channels and floodplains, while hydrological models have been used to model runoff generation from a catchment (Teng et al., 2017). Many modeling packages can now describe both the hydrology and hydraulics of drainage. Flood models/modeling are software packages that depict hydrological, hydraulic, and hydrodynamic phenomena within a catchment, such as rainfall-runoff, stream flow, and infiltration (Singh et al., 2021).

Identifying sources of flood and reducing the risk of flooding in critical areas are increasingly important aspects of flood risk management and, thus, flood modeling (Dawson et al., 2020; Fletcher et al., 2015). Recognizing the primary sources of flooding across a catchment aid in developing flood-prevention strategies (Singh et al., 2021).

Singh and his colleagues classified flood source modeling approaches into two groups: Unit Flood Response (UFR) and Adaptation-Driven Approaches (ADA). The UFR has four main steps including; 1) division of a catchment into subcatchments; 2) flood routing performance to connect subcatchments to the main outlet; 3) subcatchment response generation that compares the hydrograph from the outlet of a subcatchment with the hydrograph from the whole area; 4) ranking subcatchments based on their contribution to flood peak (Singh et al., 2021).

Saghafian et al. (2008) studied how land-use change alters the location of source areas of flood risk using UFR. They found that the largest or the closest catchments to the outlet are not necessarily the locations with high priority in runoff generation (Saghafian et al., 2008). Maghsood et al. (2019) utilized the same approach to investigate the impact of climate change on flood sources in the Talar river basin in Iran. Climate change projections increased flood sources closest to the catchment outlet in their study (Maghsood et al., 2019). Sanyal et al. (2014) applied the UFR approach by generating a baseline hydrograph for two scenarios of land uses in Konar in India. It was discovered that land-use change at a sub-catchment scale positively impacts the flood peak at the outlet (Sanyal et al., 2014).

ADA approaches not only identify the source areas but also apply sustainable urban drainage system (SUDs) measures to identify the location that benefits most from such measures in flood mitigation (Singh et al., 2021). Combined geographical information systems (GIS) and flood modeling are utilized as an ADA approach by Espino et al. (2016) to identify places most suitable for SUDs measures in Espoo, Finland. SUDs in the identified locations were modeled, and their hydrological responses were studied. According to the study, SUDs cut outflow by half inside the catchment (Jato-Espino et al., 2016). The study's findings emphasize the need to use site-specific sustainable drainage measures to improve SUDs efficiency in flood mitigation (Jato-Espino et al., 2016).

Flood models including UFR and ADA approaches can also be categorized as lumped, distributed, or semi-distributed. The complexity of a lumped model is minimized since for a certain property such as the features of soil, precipitation, and …., an average lumped value is

assigned to the whole catchment ignoring spatial variation (Singh et al., 2021). This type of model is applied in case of data limitations. In a distributed model, the catchment is divided into units, which can be zones, cells, or regions. A separate set of parameters is assigned to each unit and runoff is estimated independently for each unit. In a semi-distributed model, a catchment is divided into subcatchments to better explain spatial variation, but the internal values of parameters within each subcatchment are lumped (Pina et al., 2016). The degree to which geographic variability is accounted for is determined by the size of the subcatchments (Salvadore et al., 2015)

Hydrological models describe runoff generation. By estimating the water balance, models can estimate the peak discharge. To determine the water balance, the continuity equation is applied by a model. Hydraulic models describe the runoff path. The St. Venant equations, including both the momentum and continuity equations, can be used to compute the depth of flow and discharge downstream in a channel (Storteig, 2019).

A catchment must be defined in hydrological models to delimit the area for water intake and discharge. For surface water and groundwater studies, the catchment is recognized based on topography (Storteig, 2019); however, the groundwater may not have the same borders as the surface water (Dingman, 2015, p. 15). Due to the fact that Scandinavia's groundwater follows the topography most of the time (Beldring, 2002), a catchment based on topography can be utilized for hydrological modeling (Storteig, 2019). In addition, the flow velocity in an urban catchment is affected by the variation in Manning's roughness coefficient for different surfaces. The water is transported to an outlet faster through the sewer than through the natural flow direction on the surface. The sewer system's flow direction is crucial as it affects catchment boundaries (Storteig, 2019).

2.4 SWMM (Storm Water Management Model)

The Environmental Protection Agency’s (EPA) SWMM5 is a semi-distributed rainfall-runoff model. It models the relationship between hydrology and hydraulics, as well as the quality of runoff. The quality of the water will not be evaluated in this study. The model can also apply both UFR and ADA approach (as explained in section 2.3.1) through modeling SUDs/low impact development measures (LIDs) such as rain garden, green roof, and …. Due to time limitation, this

study focuses on the identifying flood source in the area rather than modeling LIDs. The SWMM model can simulate single events or continuous simulations (Barco et al., 2008). This study focuses on continuous simulation. This section gives an overview of the various components of the model.

2.4.1 Subcatchments and runoff

A catchment is divided into subcatchments, and each subcatchment is further subdivided into subareas of impervious and pervious (Rossman & Huber, 2016, p. 51). Each subarea generates runoff uniquely and distinctly, which means water from one subarea can reach the outflow first, rather than water from another. The reasons for this time variation are differences in properties such as Manning's roughness coefficient, depression storage, and water infiltration capacity for different subareas (Rossman & Huber, 2016, pp. 54-55). Almost immediately after precipitation reaches the surface, runoff is generated from the impermeable subarea, which lacks depression storage. The precipitation that enters the depression storage in subareas with depression is exposed to evaporation but also infiltration only for relevant pervious subareas. Runoff occurs when the depth in the depressions after evaporation and perhaps infiltration surpasses the depression storage (Rossman & Huber, 2016, p. 56).

2.4.2 Hydraulic routing model

Routing is a process that determines the downstream hydrograph based on the upstream hydrograph (Storteig, 2019). In SWMM, there are three routing options: steady-state, kinematic wave routing, and dynamic wave routing. They all apply the St. Venant equations, but in different ways. The most straightforward routing is the steady-state flow routing, which considers a uniform and steady flow. This routing approach does not alter the shape or time lag of the upstream hydrograph; instead, it simply translates it to the downstream end (Rossman & Huber, 2016, p. 36). Kinematic wave routing solves the St. Venant equations for uniform, unsteady free surface flow in a simplified form. The drawback is that it cannot simulate pressurized flow, reverse flow, or backwater effects. The approach has the advantage of allowing large time steps, which allows for more efficient computation (Rossman, 2015, p. 63). Dynamic wave routing is applied for gradually changing, unsteady free surface flow. Small time

steps applied for maintaining numerical stability are the disadvantage of this approach (Rossman & Huber, 2016, p. 40).

2.4.3 Model parameters

The width of a subcatchment, W, is the width of the overland flow in the subcatchment. In calibration, the parameter is used to optimize the shape of the hydrograph. When the subcatchment is wide, the hydrograph rises quickly, but when it is narrow, the limb rises slowly, and recession occurs (Rossman & Huber, 2016, p. 68). In a wide subcatchment, water can enter the outflow much faster than in a narrow one, resulting in an abrupt rise in the hydrograph (Bjørvik, 2021).

The subcatchment slope is calculated by dividing the difference in elevation by the distance between the points. According to Rossman and Huber (2016), the slope must reflect the dominant slope of the overland flow path to the inlet (Rossman & Huber, 2016, p. 73). The Manning's roughness coefficient, n, represents the loss of energy in open channels and is one of the most important hydrological parameters (Ye et al., 2018). For Manning's roughness coefficient, the manual recommends a range of 0.010-0.015 for asphalt, 0.040 - 0.100 for natural channels with an irregular section with pools, and 0.17 for cultivated soils (Rossman & Huber, 2016, pp. 182,184). Because imperviousness in the subcatchment is a sensitive parameter, Rossman and Huber (2016) recommend being cautious when estimating it. The amount of imperviousness for the residential catchment depends on the area of the buildings and asphalt roads.

Depression storage refers to the loss of water due to vegetation interception or surface storage. In pervious surfaces, depression storage is influenced by evaporation and infiltration, whereas depressions on impervious surfaces are influenced only by evaporation. As a result, water held in depression storage is discharged from a previous subarea faster than from an impervious subarea (Rossman & Huber, 2016, pp. 74,75). The manual suggests a range of 2.54-5.08 mm for lawn, 7.62 mm for forested litter, and a range of 1.27-2.54 mm for impervious areas as a depression storage amount. Enderney (2006), on the other hand, recommended a depression storage range of 2-3 mm in impervious roofs with slope and a range of 5-13 mm in pervious

vegetated areas (Endreny, 2006). In addition, according to Salvadore et al. (2015), when reviewing urban hydrological modeling, depression storage of 0.2-3.2 mm for impervious areas and 0.5-15 mm for pervious areas were suggested (Salvadore et al., 2015).

2.4.4 Infiltration

SWMM can model infiltration using five different methods: Horton, Modified Horton, Green-Ampt, Modified Green-Ampt, and Curve Number. This project employs the Modified Green-Ampt technique. All infiltration methods rely on factors that characterize the type and condition of the soil (Rossman & Huber, 2016, p. 86)

The modified Green-Ampt process is the same as the original Green-Ampt process with a modification. The Green-Ampt method assumes the presence of a strong wetting front in the soil column, dividing soil with some initial moisture from saturated soil. The required input parameters include the soil's initial moisture deficit, hydraulic conductivity, and suction head at the wetting front. In the modified Green-Ampt method, moisture deficit does not deplete in the top surface layer of soil at the beginning of a low rainfall period. For storms where rainfall intensity is less than the saturated hydraulic conductivity of soil, this modification can result in more realistic infiltration behavior (Rossman & Huber, 2016, p. 73).

Infiltration methods use parameters that are dependent on the soil properties in the area. Different saturated hydraulic conductivity values are provided by Rossman and Huber. According to them, the hydraulic conductivity of clay soil is 0.254 mm/h (Rossman & Huber, 2016, p. 114).

2.4.5 Groundwater

The groundwater aquifer is linked to the subcatchment in SWMM via a node known as the receiving node. For all aquifers in this study, the receiving node is the same as the outlet node for a subcatchmet. There are two zones in the aquifer: unsaturated and saturated. The upper unsaturated zone extends from the ground surface to the water table, whereas the lower saturated zone extends from the water table to the bedrock. The upper zone collects only excess rainfall through infiltration as calculated by the Green-Ampt equation. Infiltration is only modeled for the pervious subarea, whereas groundwater extends across the entire

subcatchment. Therefore, the depth of the groundwater table is considered the same across the subcatchment. Water is lost from the upper zone by evapotranspiration and percolation from the upper zone to the lower zone. Darcy's law for unsaturated flow is applied to calculate the rate of percolation. Water enters the lower zone by percolation from the upper zone and lateral groundwater flow (Rossman & Huber, 2016, pp. 136-137). Depending on the groundwater level from the bedrock in relation to the level of surface water from the bedrock at the receiving node, the saturated zone can gain or lose water through lateral groundwater flow (Storteig, 2019).

2.4.6 Precipitation and evapotranspiration

Precipitation has a maximum resolution of 24 hours and the lowest resolution of 1 minute. The intensity, volume, or accumulated unit can all be used. Each subcatchment must specify which rain gauge it gets its water from. A meteorological file with precipitation amounts for a specific period and resolution can be used in SWMM (Storteig, 2019).

SWMM uses the Hargreaves method to calculate evaporation (Rossman & Huber, 2016, p. 49). The approach is based on the temperature of the air and the latitude. A meteorological file is necessary to include temperature in the model. Each day's maximum and minimum temperatures are listed in columns in the meteorological file.

The evaporation losses are calculated from the surface of the subcatchments in SWMM. The groundwater component must be included to account for transpiration. The soil moisture lost from vegetation cover and direct evaporation of the permeable subarea is called evapotranspiration from the upper unsaturated zone. Evaporation from the lower saturated zone is referred to as lower zone evapotranspiration (Rossman & Huber, 2016, p. 134).

2.4.7 Hydraulic network components

The Hydraulic network in SWMM is mostly made up of nodes and links. The conveying element between two nodes is the link, such as a channel. The start and end points of a link are considered nodes. In other words, each node is a connection between two links, such as a junction between two channels (Rossman & Huber, 2016, p. 31). The type of node can also be a storage type referred to as a storage unit. Storage units are nodes in the drainage network that

provide storage space (figure 2-2). They could be as small as a tiny basin or as large as a lake in terms of physical size. A function or table of the surface area against height describes the volumetric features of a storage unit (Rossman, 2015, p. 50). A storage unit can be used in a location within a network where there is depression, such as a lake in the water flow path/link and hence associated adverse (negative) slopes.

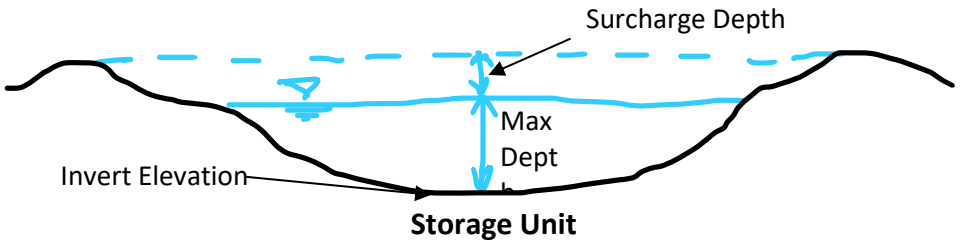

Figure 2-2: The schematic illustration of a storage unit with invert elevation (bottom elevation), maximum depth, and surcharge depth. The figure is inspired by the SWMM reference manual-Volume II.

The link can have the geometry that the user chooses, either by following SWMM's options or by creating a custom shape. The geometry of the linkages affects whether they are open or closed. Links only transmit water between nodes, but if the user specifies a loss value, the links can drain a steady amount of water into the soil (Rossman, 2015, p. 33).

2.4.8 Calibration, validation, and continuity error

Calibration of a model is critical to assure the model's quality. Typically when calibrating, observed data are compared to model-generated and simulated values. The model's parameters are modified to get the best feasible correlation between simulated and observed data (Bjørvik, 2021). Initial estimates of the parameters are required for physically based rainfall-runoff models (Barco et al., 2008). One method is manual calibration which can be carried out by trial and error. This method is time consuming, labor intensive particularly when the catchment is complex and large in area and allows for interpretation that might be wrongful. Another calibration method is automatic optimization, which applies mathematical algorithms to find the least discrepancy between observations and simulations (Barco et al., 2008). However, the approach may disobey physical principles, and in an attempt to compensate for faults, it may generate implausible parameter values (Bjørvik, 2021).

Numerical errors are associated with numerical methods. Continuity error or mass balance error is an essential factor showing the health of a model in SWMM (Meng, 2021). This error which is in percentage appears once running the model ends, showing both runoff continuity error and hydraulic continuity error (Dickinson, 2010). A runoff continuity error is calculated with equation 2.2 (Dickinson, 2010).

Continuity error = 100.0 * (1.0 - Total outflow/Total inflow) (2.2)

Where:

Total inflow = Rainfall+ Initial storage + initial snow cover

Total outflow = Evaporation + Infiltration + Runoff + Snow removed + Final storage + Final snow cover.

A hydraulic continuity error is estimated in the same way based on inflow and outflow, except it can be included in more ways for water to enter and exit from the network, such as dry weather inflow into the network and outflow from the outlet. This error shows the amount of water in percentage lost from the routing, resulting in a negative value, or gained by the routing, resulting in a positive value (Dickinson, 2010).

Continuity error can be relevant to both system and junctions. After simulation, nodes with larger error values should be reviewed (Meng, 2021). When the continuity error is poor, the error should be reached an acceptable range which is between -5% and +5%. A continuity error of zero shows a very reliable model (Dickinson, 2010).

2.5 Flood map

The results of the hydrological and hydraulic models might be overwhelming to a non-technical user. Nonetheless, these results can be applied in a GIS framework by doing the necessary spatial analysis to generate flood maps that are simple enough for the public to grasp. Flood maps are a useful tool to communicate flood features to the public and users and are thus regarded as the main initial step in flood risk management (Adhikari, 2020). Flood maps are classified into two types based on their content, purpose of usage, accuracy, and user's target: flood inundation maps and flood risk maps (Adhikari, 2020). In this study, flood inundation maps

were produced. Flood inundation maps are the product of a process that includes hydrological, geospatial, and hydrodynamic analyses to display flood parameters such as (i) the level of inundation, (ii) the intersection of the flood level with the terrain (generating flood extent), (iii) flood depth (the difference between the flood level and the terrain) (Adhikari, 2020).

3 Study area and background

The study area of this thesis is the Sogn allotment garden, as well as the adjacent areas to the west and south of the allotment garden, located in the lower parts of Gaustad catchment in Oslo (Figures 3-1 and 3-2)

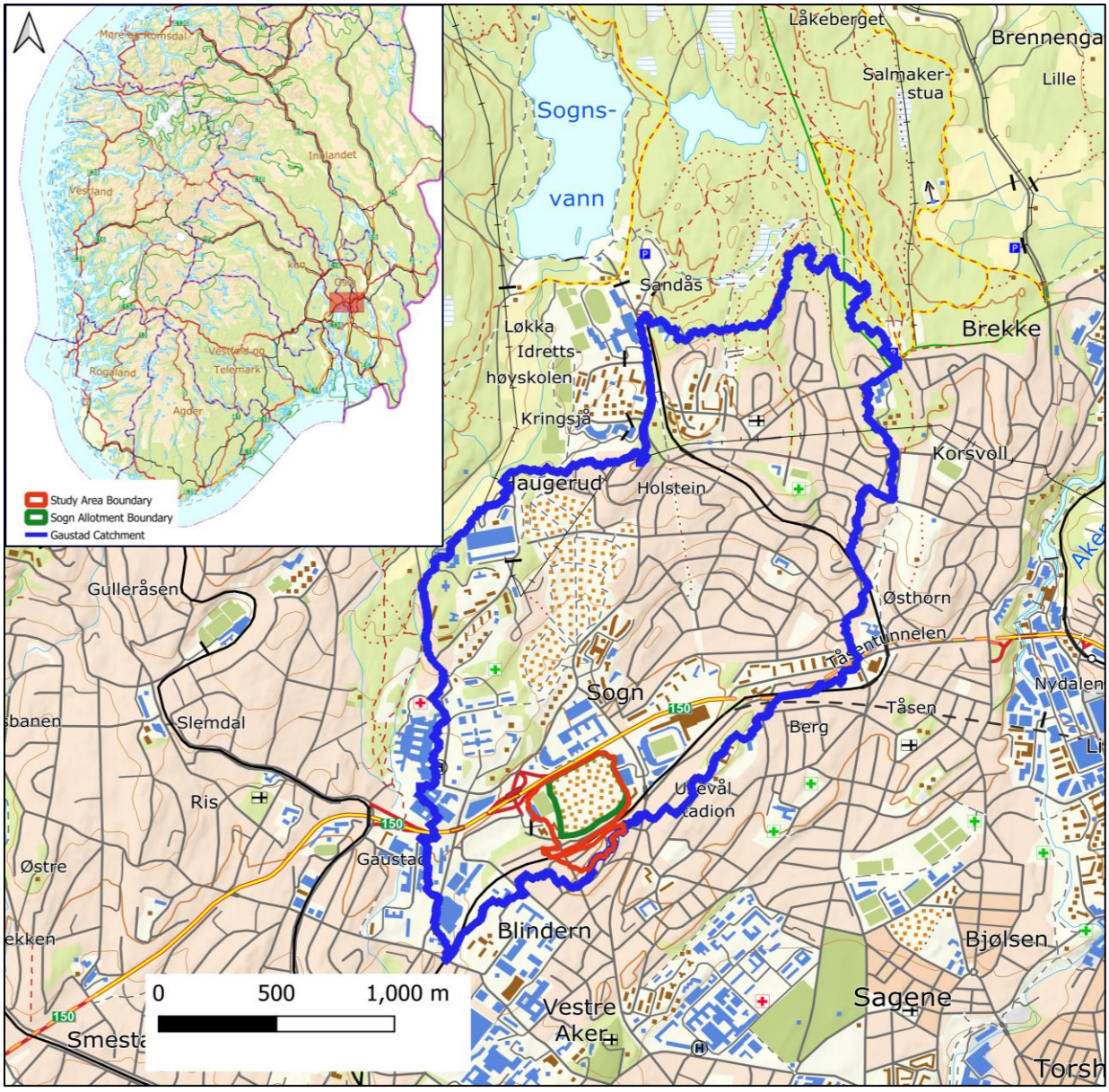

Figure 3-1: The study area including Sogn allotment garden and its adjacent areas located in the lower parts of the Gaustad catchment in Oslo. The map was made in QGIS. The background map is from the Norwegian Mapping Authority ©Kartverket

The Sogn allotment garden is characterized by parcel gardens, cabins, gravel roads, an asphalt road, and a parking space. The nearby parts of the allotment inside the study boundary are characterized by student housing, a football pitch, residential houses, and asphalt roads (Figure 3-2). The total area of the study site is 15.2 ha. with the allotment garden taking over 8.70 ha.

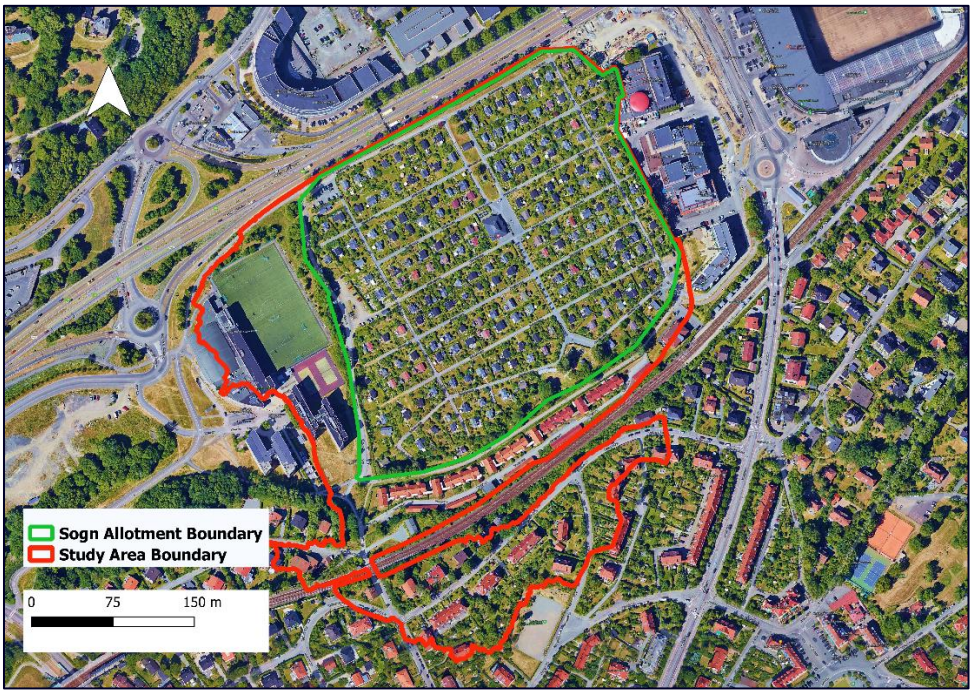

Figure 3-2: Sogn allotment garden and adjacent areas that contribute to runoff towards the allotment. The background map is from google maps.

3.1 Background

The Sogn allotment garden consists of 204 plots of gardens; each has a small cabin. The allotment garden was once established as a green lung and living park for their surroundings. Today in line with Oslo municipality's strategy in water management (as explained in the introduction), investigation of the role of the allotment in flood mitigation is the relevant topic (NIVA, 2018). The Sogn allotment garden is a green area that also offers natural retention in an urbanized area. Nevertheless, the site and locations within the allotment garden are also prone to stormwater inundation due to runoff generated within the garden itself and the surrounding area's characteristics. The garden is exposed to surface runoff inundation during heavy rains.

The Sogn allotment garden is currently also being used as a site for researching nature-based solutions for stormwater management (NIVA, 2018).

According to a study by NIVA in 2018, based on an online survey, some locations within the allotment were identified as water accumulation spots and were marked on the map by the allotment residents (Figure 3-3).

Figure 3-3: Water accumulation spots based on residents' observation from an online survey by NIVA in 2018 (Red / orange core means a high concentration of markings). The map is from the Sogn allotment report on NIVA's website.

The red/orange cores in figure 3-3 show the accumulated stormwater concentration, which is mainly to the west and at the center of the allotment. They also show the locations where water stands for more than two days. According to the residents' recall, at the spots on gravel roads scattered over the garden, the water did not accumulate larger than 8 or 9cm (NIVA, 2018). However, there is not any measurement of water depth provided by residents for the spots on the map in general.

At the location shown with the red/orange color at the center of the allotment in figure 3-3, two rain gardens were identified when a field visit was done. These two rain gardens were built recently, and their function is to drain the accumulated water at the center through a pipe to a point on the south side of the allotment garden. Furthermore, at the east of the allotment,

where there is another red/orange mark on the map, a wetland has been built to drain accumulated water from this area. However, no such mitigation measures are performed yet for the rest of the area. The Sogn allotment garden has no drainage system and is not connected to the stormwater drainage system of the surrounded area. There is a drainage system to the north from a ring road and to the east from a parking lot, right next to the allotment. The drainage facilities (inlets) in these two parts work as a divide and separate the study area from the stormwater drainage system (based on the field visit which will be discussed in section 4.3). There are also no rivers or open streams in the area. Historically, there were two rivers to the west and south of the allotment which are now in the underground pipes (Bjørvik, 2021). Nevertheless, the area is not connected to these pipes (Personal communication with co-supervisor/NIVA).

3.2 Climate

The climate of Oslo is humid continental which results in warm and humid weather during the summertime and cold weather in the wintertime (Peel et al., 2007). The Blindern station, 94 meters above sea level, located approximately half a kilometer to 1 kilometer away from the allotment garden, is the closest meteorological station (NIVA, 2018). At Blindern (18700), the average annual rainfall has been 884 mm throughout the last five years (2017-2021). During the same time frame, the average air temperature was 7.5 °C yearly (Norwegian Center for Climate Services, 2022)

The climate in Oslo, like the rest of Norway, is warming, and the long-term outlook implies that adaptation is required (Moheseen, 2015). The climate profile of Oslo was revised in January 2021, presenting a review of the current climate status and future issues as provided in the IPCC Fifth Assessment Report (AR5). The climate profile is designed to be applied as a guide for making climate adaptation decisions, infrastructure dimensioning, and risk analysis (Bjørvik, 2021). A higher amount of precipitation in Oslo is likely to result in a high stream and river discharge (Bjørvik, 2021).

In Oslo, the annual precipitation is anticipated to grow by 15%, from the baseline 1971-2000 to 2071-2100. When dimensioning for rainfall occurrences shorter than 3 hours, a climate

surcharge of 40% is recommended as a general guideline (Bjørvik, 2021). Similarly, the mean temperature is predicted to rise about 4°C, with the greatest change occurring during the winter, causing the growing season in Oslo to be extended by about two months (The Norwegian Centre for Climate Services (NCCS), 2017).

3.3 Geology

The bedrock in the study site consists of limestone, shale, and marl (Geological Survey Of Noway (NGU)). The loose masses over the bedrock in the area mainly consist of marine deposits (Figure 3-4, b). As figure 3-4.a shows, the infiltration capacity in the area of the allotment is mainly mapped as “not suited for infiltration” (Geological Survey Of Noway (NGU)). Clay is generally considered to have limited or very poor infiltration capacity (NIVA, 2018), which is assumed for the area with “not suited for infiltration” classification.

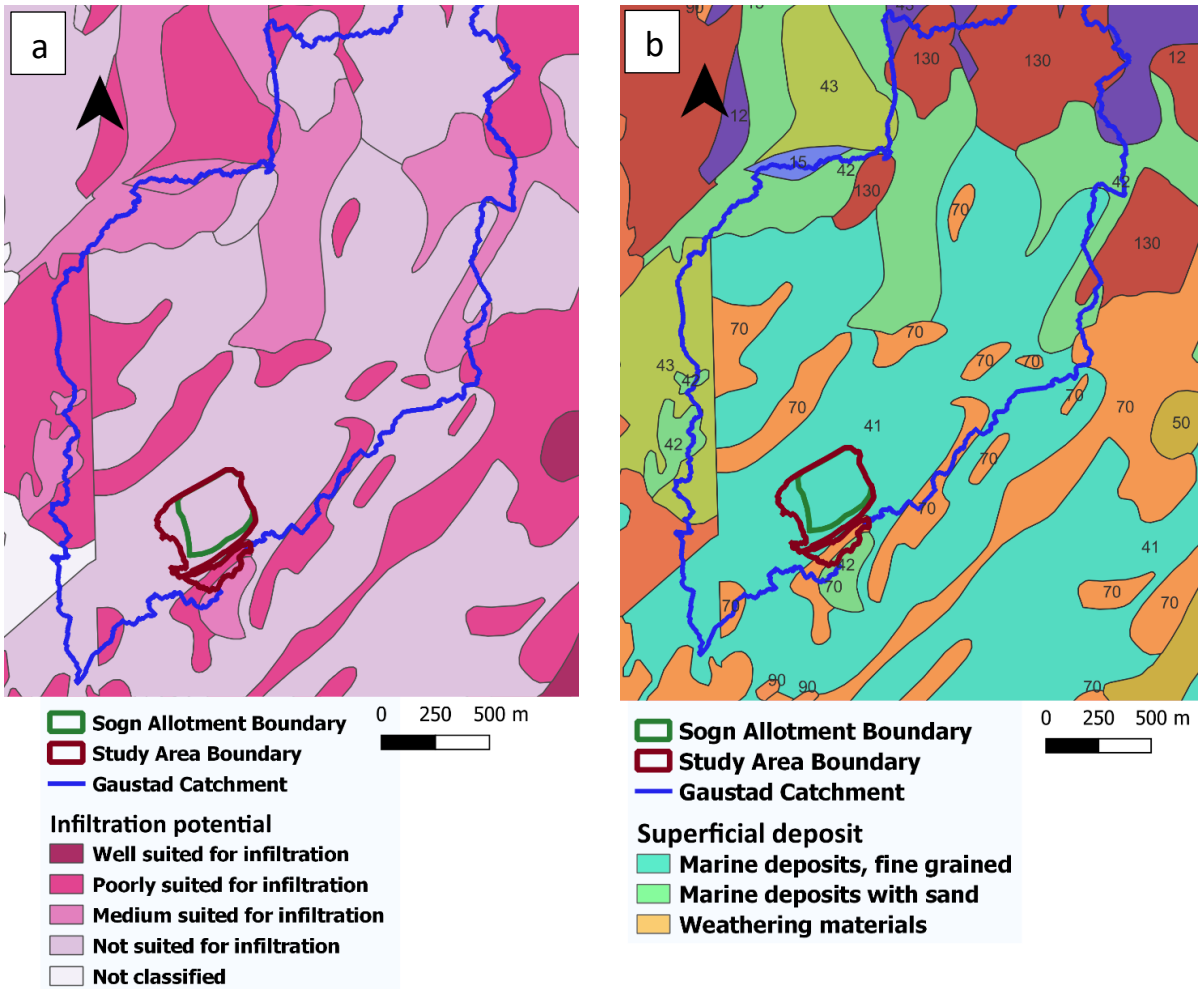

Figure 3-4: Infiltration capacity (a) and deposits (b) at study site. Data from the Norwegian geological survey (NGU), maps were created in QGIS.

4 Method

4.1 Data collection

The initial phase for setting up the model was to acquire the required data and information. Table 4.1 shows the data files that were used in the thesis, as well as their source and aims.

Table 4.1: Data files used in the thesis, as well as their source and aims

ID	Type of Data	Source	Objective
1	Digital Terrain Model (DTM)Map	høydedata.no	To obtain the subcatchments slop, and to generate streamlines based on topography in GrassGIS, to define the geometry of the transects across the identified channels in SWMM
2	Building map	geonorge.no	To add the building condition to the DTM layer and obtain surface streamlines in GrassGIS
3	Land Use Map	geonorge.no	To estimate the pervious and impervious subareas within each subcatchment, to analyze the flood sources and inundation
4	Precipitation	(Norwegian Center for Climate Services, 2022)	To import as an external file for the analysis of the runoff in SWMM throughout 01.01.2017-25.02.2022
5	Temperature	(Norwegian Center for Climate Services, 2022)	To import as an external file for the analysis of evaporation in SWMM throughout 01.01.2017-25.02.2022
6	Scientific journals, scholarly articles, SWMM manual, books, reports etc.	HVL library, web of science, and other online sources	To gain knowledge in flood analysis, to provide guidance while setting up the model, and to refere in different sections

4.2 GRASS GIS and delineation of subcatchments

The subcatchments in the study area were delineated using the Geographic Resources Analysis Support System (GRASS)GIS, version 7.8. GRASS GIS is a free and open-source data management and image processing program developed by the United States Army. A Digital Terrain Model (DTM) map with a resolution of 1m*1m was chosen for this study. To generate streamlines, the software requires a DTM as an input file. In addition, a building map was added to the layer of DTM in GrassGIS since the buildings and infrastructures can alter the flow paths. The streamlines based on the topography and building conditions were generated (Figure 4-1). The outlet of the catchment was identified based on the streamlines. The initial catchment and the related subcatchments associated with the identified outlet covered a large area in Gaustad catchment (Figure 4-2). The catchment border was then altered based on a site visit and additional investigation, as stated in the following section.

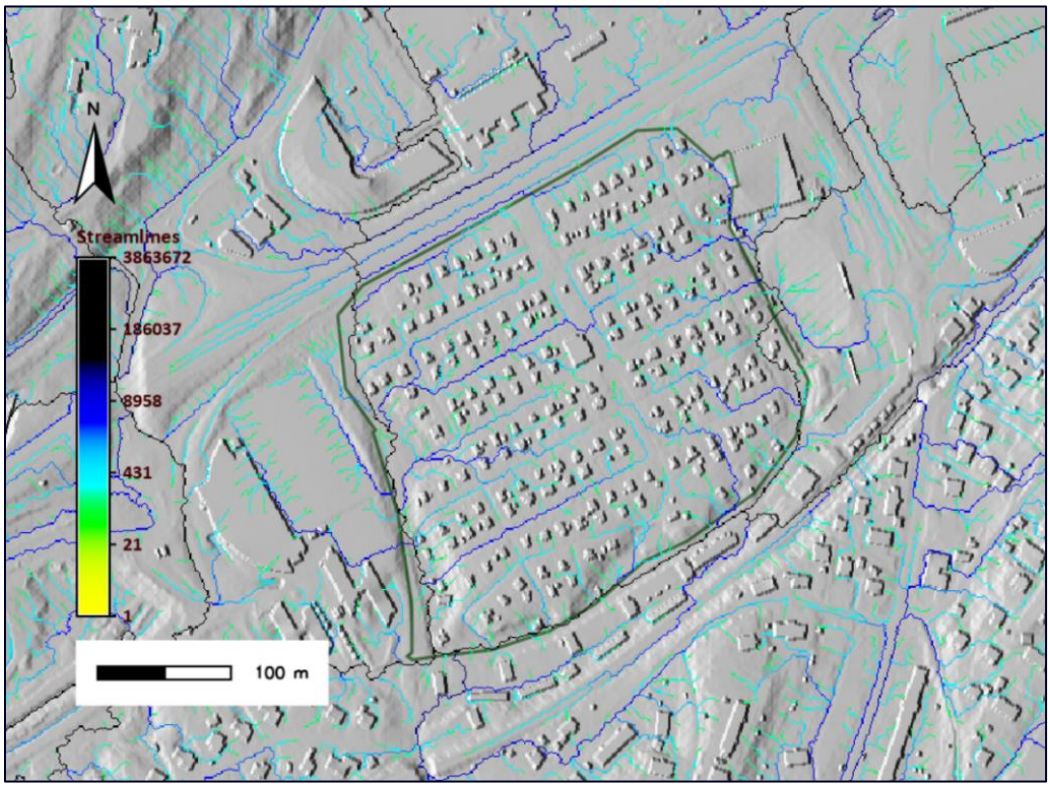

Figure 4-1: Streamlines over the DTM and building map; the darker flow lines show the larger branches of the stream, and the lighter show, the smaller branches. The green line shows the boundary of the Sogn allotment garden. The map was made in GrassGIS.

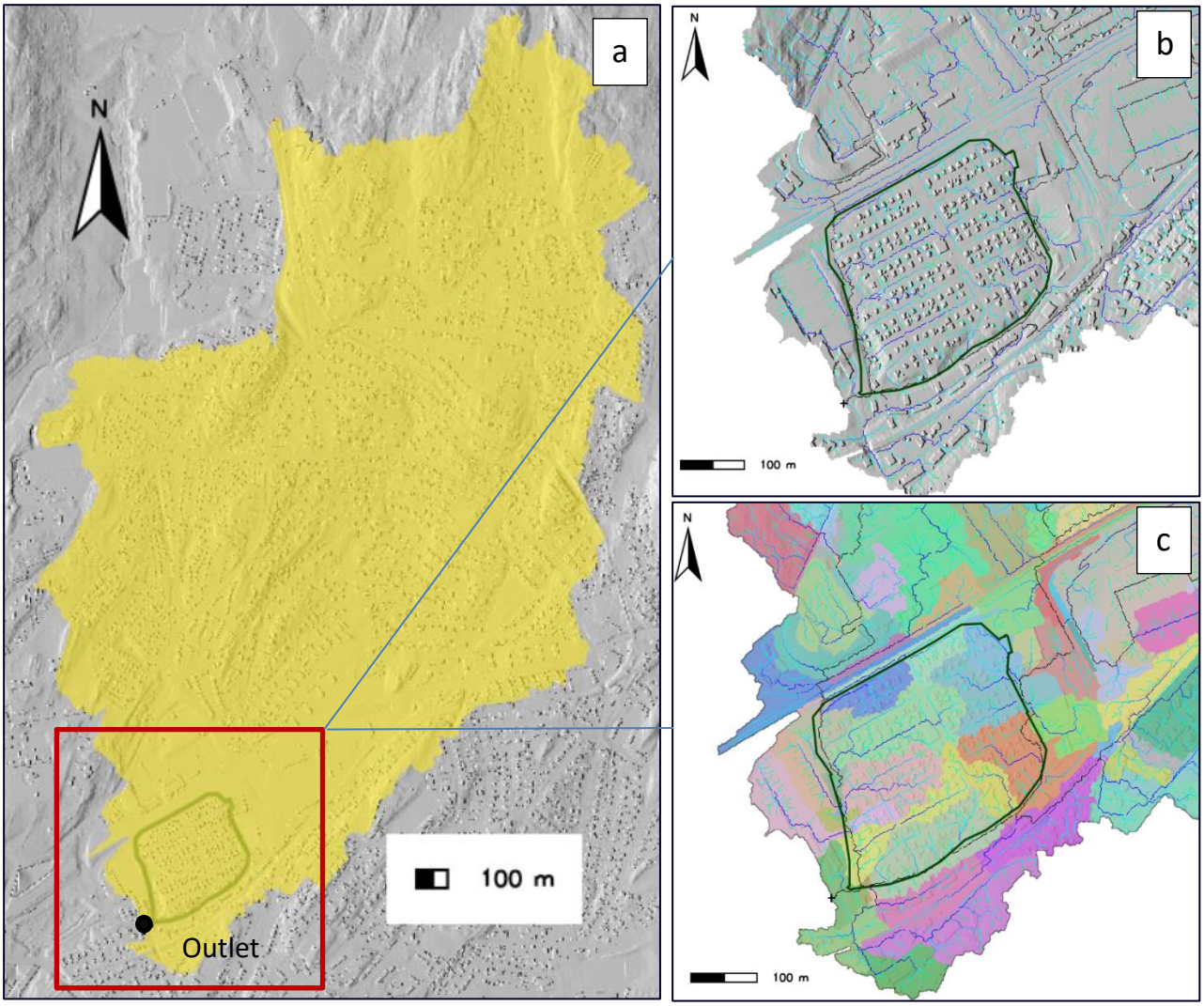

Figure 4-2: a) Initial catchment and the outlet, (b) associated streamlines and c) initial subcatchments based on the streamlines. Colourful shapes show the subcatchments. Green line shows the boundary of the Sogn allotment garden. The black point shows the identified outlet. The maps were made in GrassGIS

4.3 Field visit

A field visit was done with the aim of investigating the condition of the study region, finalizing the catchment area to the chosen outlet, and defining the final flow pathways. During the field visit, the stormwater drainage inlets around the allotment were identified (black dots in figure 4-3). Based on this identification, those parts of the surrounded areas connected to the stormwater drainage system through inlets were excluded. The runoff from these areas does not flow towards the allotment. As a result, only areas that were not connected to the

stormwater drainage system remained as the final study area (inside the red boundary in figure 4-3).

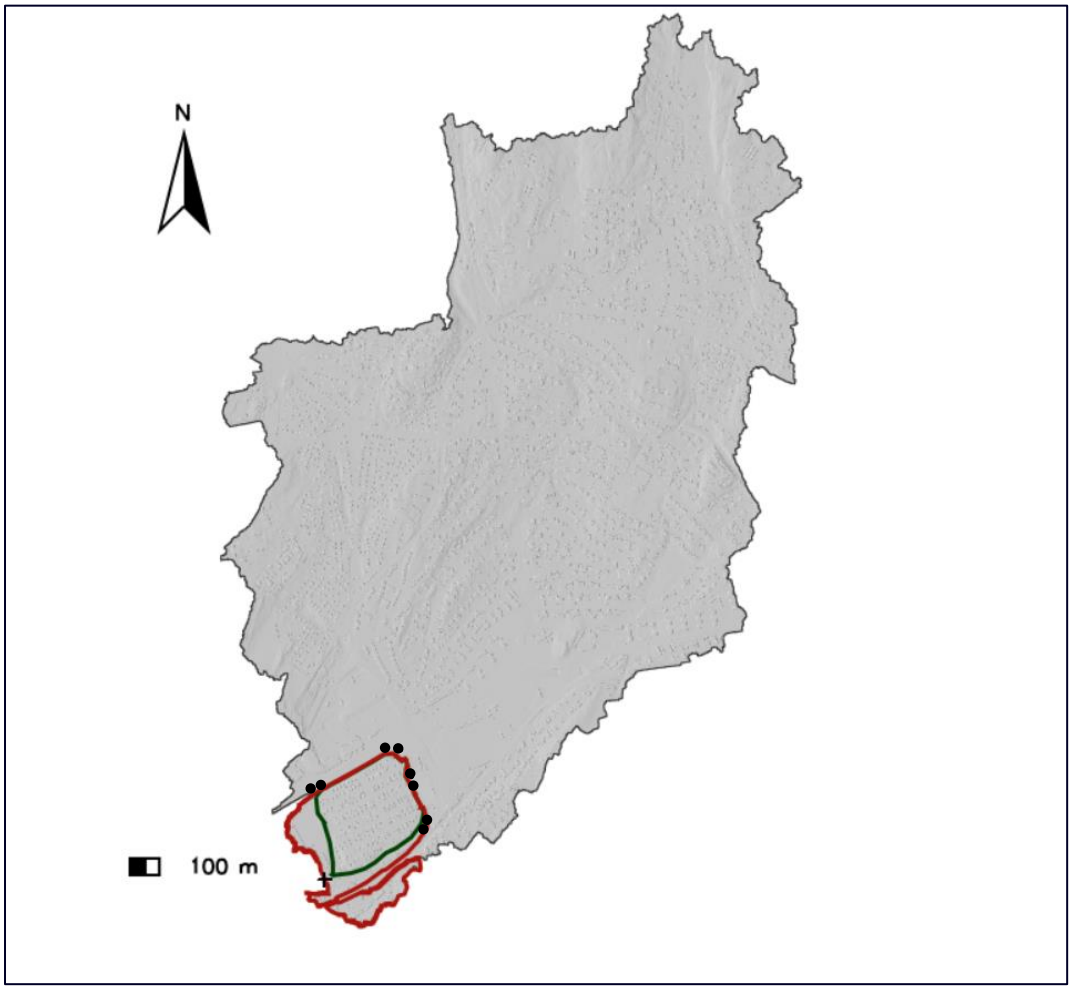

Figure 4-3: Final boundary of the study area (red boundary) within the initial catchment (grey boundary). All the areas outside the red boundary were excluded from the initial catchment. Black dots show the identified inlets of the stormwater drainage system. The green boundary shows the Sogn allotment garden. The map was made in GrassGIS.

4.4 QGIS, finalizing subcatchments

The raster layer of the streamlines and the polygon layer of the initial subcatchments from GRASSGIS were imported into QGIS for finalizing the subcatchment delineation. Based on the DTM map, the associated contour lines, streamlines, and observation of the terrain condition through the field visit, two main channels were identified in the study area (Figure 4-4). The

study area drains into these two channels, which are then combined before the final outlet to form one large channel that encompasses the outlet.

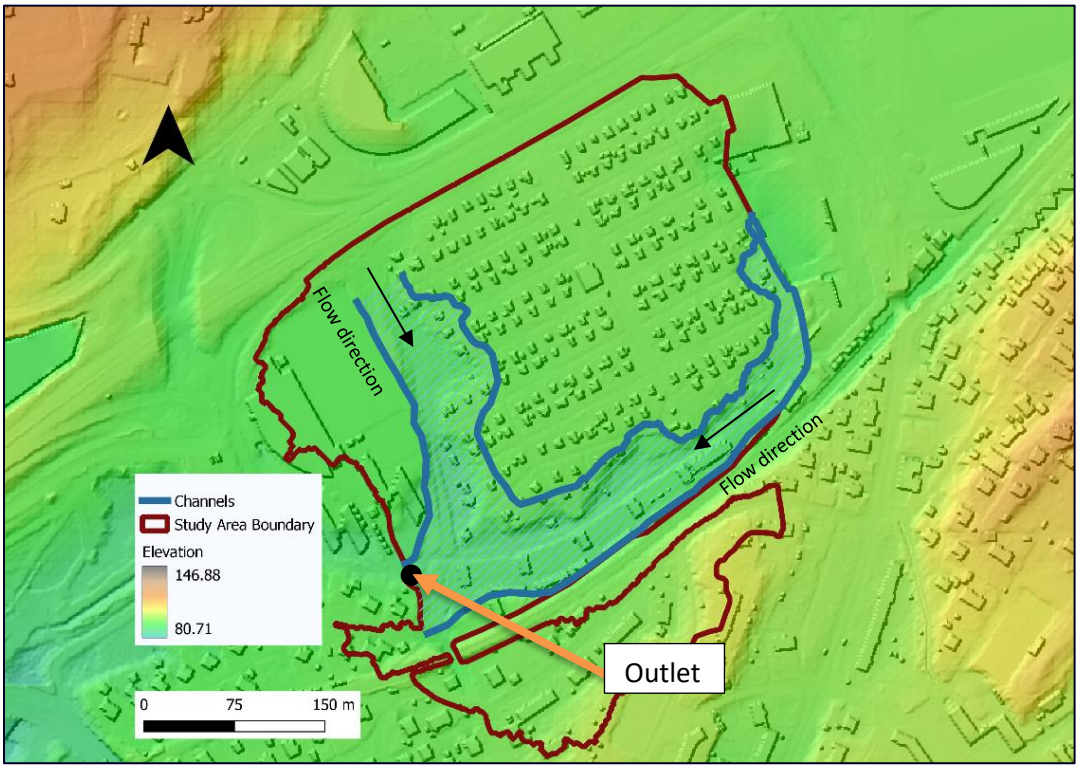

Figure 4-4: Identified channels in the study area. The background layer is hillshade DTM map showing the surface elevation from sea level in meters. The map was made in QGIS.

The channels were used for the final delineation of the subcatchments. Within the boundary of the study, every subcatchment without a direct outlet to the channels was merged with its neighbor subcatchment that had a direct outlet to the channels. Therefore, all the final subcatchments drain into the channels. 22 subcatchments were finalized for further analysis. The final study area (the allotment garden and the identified adjacent areas), including 22 subcatchments, are illustrated in figures 4-5 and 4-6.

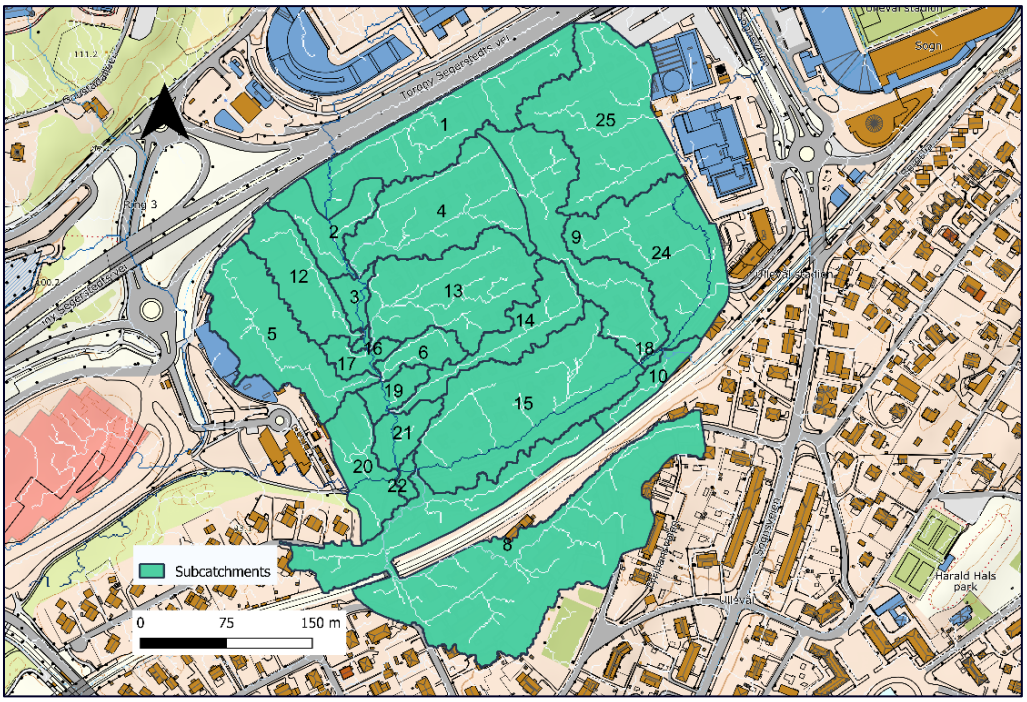

Figure 4-5:Final subcatchments of the study area as well as the streamlines within the subcatments. The map was made in QGIS.The background map is from the Norwegian Mapping Authority ©Kartverket

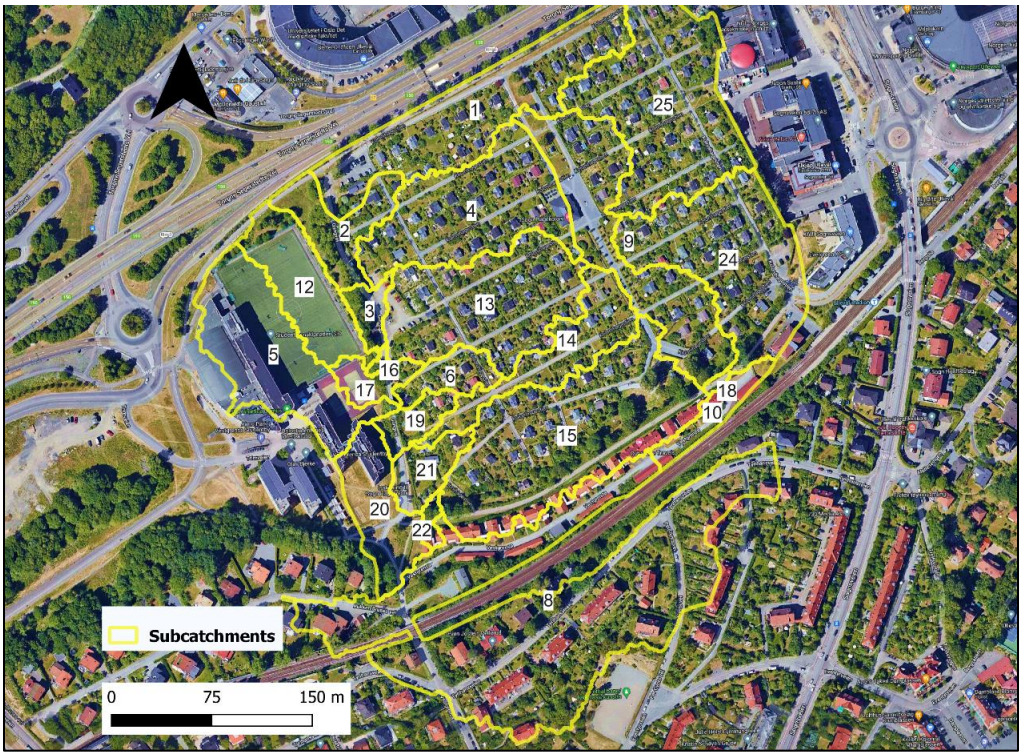

Figure 4-6: Final subcatchments of the study area. The map was made in QGIS. The background map is from google maps

4.5 Terrain analysis

The terrain analysis was carried out in QGIS to acquire the area, slope, and width of each subcatchments as input for the model. The area and width of the subcatchments were measured from the subcatchment polygon layer. The average slope from the DTM raster layer was obtained using the profile tool and further calculations in Excel. The average slope of each subcatchment was determined by measuring the average slope of the profile along each subcatchment's main streamline. The area of pervious and impervious surfaces in each subcatchment was also estimated using the land use map. The areas of the cabins, asphalt roads, and other buildings were considered impervious subarea in each subcatchment.

4.6 Model setup in SWMM

The model was set up using EPA SWMM software, version 5.2, to analyze the dynamics of the runoff by continuous simulation from 01.01.2017 to 25.02.2022. The model considers both surface runoff and groundwater.

4.6.1 Subcatchment’s parameters

The vertices of the subcatchments were exported as a CSV file from QGIS. The vertices were further adjusted in Excel to make them readable by the SWMM software. The adjusted vertices were loaded into SWMM's input file. The parameters of 22 subcatchments used for the model setup are provided in tables 4.2 and 4.3. The parameters of area, width, average slope, impervious fraction, and Manning’s number for overland flow were assigned to each subcatchment separately (table 4.3, A.1). The rest of the parameters shown in table 4.2 are the same for all subcatchments.

Table 4.2: Definition and values of subcatchment parameters/properties

Subcatchment parameters	Definition*	Value
Outlet	The node or subcatchment name that receives runoff from an existing subcatchment.	Table 4.3
Area (ha)	The subcatchment area encompassed both permeable and impermeable areas.	Table 4.3
Width (m)	The width of the runoff flow path in existing subcatchment	Table 4.3
%Slope	The subcatchment's average percentage slope	Table 4.3
%Imperv	Impervious surface area in percent	Table 4.3
N-Imperv	Manning's n for runoff over impervious areas within subcathment	0.012
N-Perv	Manning's n for runoff over permeable areas within subcatchment	Table 4.4, A.1
Dstore-Imperv (mm)	The depth of depression storage on impervious areas within subcatchment	1.9
Dstore-Perv (mm)	The depth of depression storage on pervious areas within subcatchment	5.08
%Zero-Imperv	Percentage of impermeable areas that do not have depression storage	100%
Subarea Routing	Impervious: runoff from pervious areas flows to impervious Pervious: runoff from impervious area flows to pervious area Outlet: runoff from both areas flows directly to an outlet.	Pervious
Percent Routed	The percentage of runoff that is routed between subareas.	100%
Suction head (mm)	The average value of soil capillarity suction along the wetting front	320
Conductivity (mm/h)	Soil saturated hydraulic conductivity	0.254

*Source: (Rossman, 2015, pp. 196, 232)

Table 4.3: Values of subcatchment parameters specified for each subcatchment

Subcatchment ID	Area(ha)	Impervious area (%)	Width(m)	Average slope (%)
S1	1.1435	9.38	39.20	1.19
S2	0.3713	2.90	33.50	4.52
S3	0.1188	12.03	20.57	1.67
S4	1.0196	13.26	51.10	2.59
S5	0.9198	57.40	39.75	3.05
S6	0.1901	15.45	19.75	7.97
S8	3.0852	36.00	60.77	4.64
S9	0.9817	10.22	34.16	2.40
S10	0.1843	39.17	19.22	3.55
S12	0.5279	0.00	33.49	3.40
S13	1.0685	13.27	53.04	3.31
S14	0.5003	18.16	21.28	4.05
S15	1.5783	24.54	66.91	3.03
S16	0.0203	31.62	9.71	1.17
S17	0.1461	7.01	25.26	8.74
S18	0.0190	35.31	8.40	1.83
S19	0.1539	18.29	40.26	13.53
S20	0.4418	36.42	40.54	4.18
S21	0.2095	17.46	35.47	8.14
S22	0.0481	67.68	12.74	4.34
S24	1.1342	19.74	45.47	2.42
S25	1.3206	13.00	57.87	1.78

The values of the Manning's number (n) and the depth of depression storage related to pervious and impervious subareas were chosen based on the type of land cover from the tables by Rossman (Rossman, 2015, pp. 181-182). The depression storage depth for impervious and

pervious surfaces was chosen as 1.9 and 5.08, respectively. Manning's values based on the type of land cover are shown in table 4.4.

In SWMM, regarding Manning's n, one value for the pervious area and one for the impervious area can be assigned to each subcatchemnt. Manning's number for the pervious subarea was estimated separately for each subcatchment. The average value of the Manning's n of different pervious land covers based on their area within each subcatment was calculated and assigned to the same subcatchment (Table A.1).

Manning's number for impervious subareas was the same for all subcatchments. According to Rossman (2015), there is the same value of the roughness number for both asphalt roads and roofs, and hence no need to estimate the average value based on the area of each type of land cover. The value was chosen as 0.012 according to Rossman (Rossman, 2015, p. 182).

Table 4.4: Manning's number (n) for overland flow based on the land cover in the study area

Land type	Garden*	Asphalt road	Roof	Gravel road**	Natural area
Manning's roughness number(n)	0.17	0.012	0.012	0.02	0.13

*Garden's n was considered as cultivated soil with residue cover > 20% from the table proposed by Rossman (2015) (Rossman, 2015, p. 182).

**Source: (Dickinson, 2002)

The soil type was assumed to be clay based on NGU's infiltration potential map. The modified Green-Ampt method, as described in section 2.4.4, was chosen as an infiltration method for this study. The hydraulic conductivity and suction head parameters for the Green_Ampt method were selected based on the type of soil (clay) according to Rossman and Huber (Rossman & Huber, 2016, p. 114).

4.6.2 Hydraulic network compartment (nodes and links)

The nodes (junctions and storage unit) and links (conduits) were made in SWMM. The outlet of each subcatchment and the points in which the channels change in width and elevation were considered junctions. The elevation of the nodes was obtained from the DTM layer in QGIS and then was assigned to them in the model. The type of conduits in this model is the open channel. As explained in section 2.4.7, conduits are characterized by two nodes (the inlet and outlet nodes), length, and a transect that defines the conduit's geometry. The length of each conduit was estimated based on the length of the streamline between two sequent junction nodes measured in QGIS. 24 transects in total were made and assigned to 24 conduits. A transect includes geometric data that explains how bottom elevation changes with horizontal distance in a cross-section of an open irregular-shaped conduit (Rossman, 2015, p. 50). Only one transect can be assigned to each conduit. 24 cross-section profiles were made across the channels in QGIS (Fig. 4-7) to define the transects in SWMM. As an example, one of the transects after construction in SWMM is illustrated in figure 4-8. The station and elevation values for each transect are based on the elevation and distance values obtained from the DTM layer in QGIS, as shown in figure 4-8. Then the values were imported into the SWMM model.

Figure 4-7: Transect profiles across the channels and the storage unit location. The colorful lines show the transects across the channels. The map was made in QGIS.

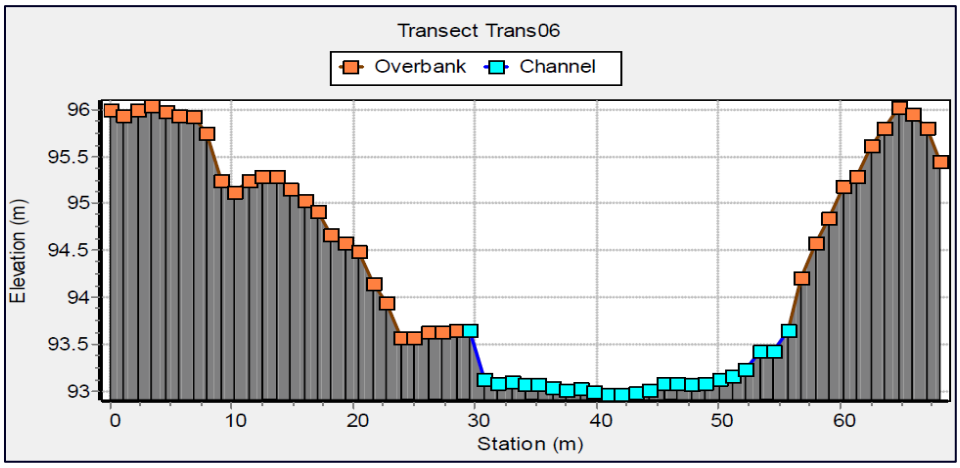

Figure 4-8: Illustration of an example of the transects made in SWMM.

The left and right banks and the main channel were defined for each transect. Then, Manning's roughness number (n) was assigned to each transect. The Manning's n in this study is varied in the channel's left, center, and right because there are different land covers in each part. The average Manning's n based on the type and area of the land cover on the left, center, and right of each transect was calculated. The values of n (table 4.5) based on the land cover and for open channels were optained from the table by Rossman (Rossman, 2015, p. 184) .

Table 4.5: Manning's roughness number(n) for open channel and flood plain based on the land cover in the study area

Land cover type	Asphalt/concrete	natural irregular channel	building
Manning's n	0.015	0.04	0.1

The results of Manning's n estimation for all conduits and associated transects, including left and right banks and the center of the transects, are shown in table A.2.

Initially, for this master thesis, a model with 44 conduits and 45 junction nodes was made. Then that model, which included some conduits with adverse slopes, was changed to the current final model. In the final model with 24 conduits and 23 nodes, the areas in depression were considered as a large "storage unit" node, as shown in figure 4-7. As a result, the conduits with

the adverse slope in the initial model were removed, and the subcatchments that drained to the depression junctions were now drained to the storage unit. In section 6.2, the reason for this change will be discussed in more detail. Based on the topography and condition of the site, a tabular storage unit with a bottom area of near zero and a higher area of 10507 m2 at a depth of 2.63 m was chosen to cover all areas in depression. Figure 4-9 shows the model network, including 24 conduits, 22 junctions, one storage unit, and their locations in the subcatchments.

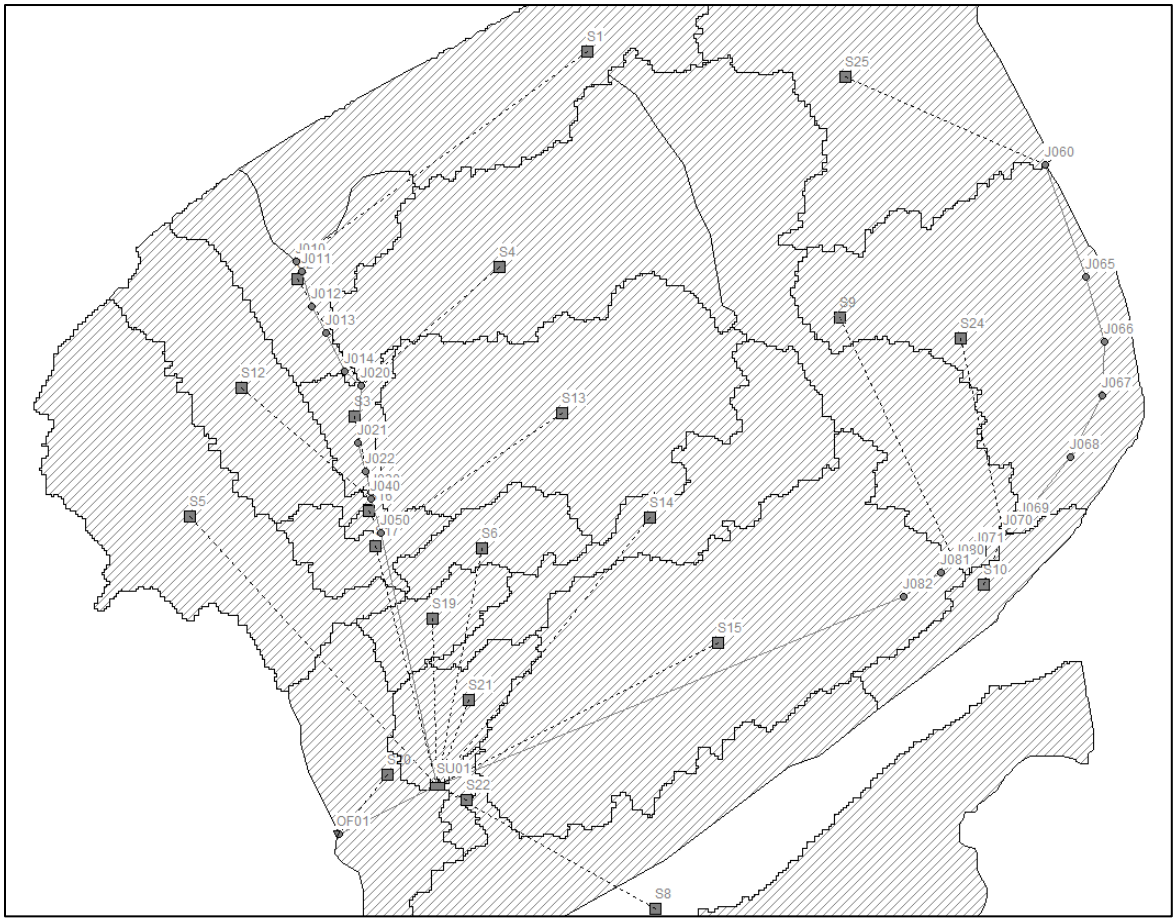

Figure 4-9: Illustration of the model's hydraulic compartment, including nodes and junctions and its overall layout in the model. Black dots with the prefix J represent the junctions. The solid black line between two junctions shows a conduit. SU01 is the storage unit. Black squares with the prefix S represent subcatchments.

4.6.3 Meteorological data

A rainfall time series from 01.01.2017 to 25.02.2022 with 10 min resolution in the form of a".dat" file was inserted into the model. Rainfall data from the Blindern (SN18700) gauging station was obtained from the Norwegian Center for Climate Services and the recorded

temperature for the same period. The daily maximum and minimum temperature .dat file was also imported into the SWMM. The precipitation used as input was considered to fall evenly distributed across the entire area. Evaporation was estimated based on the daily air temperature from the external temperature file.

4.6.4 Groundwater parameters

SWMM can assess groundwater flow for each subcatchment separately. For each subcatchment with a separate outlet, an aquifer can be defined. However, for the subcatchments with a common outlet, the same aquifer can be assigned. Each groundwater aquifer can have distinct features and elevations that are linked to a subcatchment. Except for the surface, bottom, and groundwater elevation (table 4.7), the properties of all aquifers are the same in this study (table 4.6).

The parameters of porosity, wilting point, field capacity, and conductivity were modified based on proposed values in Rossman and Huber based on the type of soil (Rossman, 2015, p. 178; Rossman & Huber, 2016, p. 178) (table 4.6).

The rest of the parameters were set as default values unless they needed modification due to unit differences.

Table 4.6: Aquifer and groundwater flow parameters definition and values for the study area

Parameters	Definition*	value
Porosity	Volume of voids/Total soil volume	0.479
Wilting Point	Soil moisture content where plants cannot extract water from the soil	0.265
Field Capacity	Soil moisture content after gravitational drainage	0.378
Conductivity (mm/h)	The saturated hydraulic conductivity of the soil in the aquifer	0.254
A1 [-]	groundwater coefficients in groundwater lateral flow equation	1
B1 [-]	groundwater coefficients in groundwater lateral flow equation	1
A2 [-]	groundwater exponents in groundwater lateral flow equation	0
B2 [-]	groundwater exponents in groundwater lateral flow equation	0

*Source (Rossman, 2015)

The surface elevation at the outlet of each subcatchment is determined using the elevation from the DTM map. In the absence of measured data for bedrock depth in the study area, the values of the bedrock elevation (bottom elevation) for the subcatchments were estimated based on the average bedrock depth in the vicinity of the research region. The bedrock depth in the vicinity was obtained from the borehole map for Oslo from geonorge.no. The borehole map, including the depth of bedrock in the existing boreholes in Oslo, did not cover the study site. The bedrock depth varied between 0 and 40m for the closest boreholes to the study site. The same variation was observed in the map for the whole of Oslo. Therefore, the average value of 20 m was used to estimate bedrock elevation for different aquifers further.

The groundwater elevation should be assigned to the aquifers as the initial groundwater condition in continuous simulation. The initial groundwater elevation was estimated based on the difference between the surface elevation and the groundwater depth. In the absence of measured groundwater depth at the start of the simulation period, the recorded groundwater depth from three data loggers in the research region from 18.12.2021 to 30.03.2022 was used. The data are from the same season as the start of the simulation period. However, this might differ from the actual groundwater condition at the beginning of the simulation period. The average groundwater depth with a value of 1.06 m was estimated from the groundwater depth recorded by all loggers throughout the recording. The loggers were close to each other and located in subcatchment9. There was no recorded groundwater depth for the other locations in the study site.

Table 4.7: Groundwater elevation at nodes and associated subcatchments and aquifers as well as relevant surface and bottom elevation

Subcatchment ID	Aquifer ID	Node ID	Surface elevation at node (m)	Bottom elevation at node (m)	Groundwater elevation at node (m)
S1	A1	J010	94.85	74.85	93.79
S2	A2	J020	92.97	72.97	91.91
S3	A3	J030	92.18	72.18	91.12
S4	A2	J020	92.97	72.97	91.91
S5	ASU01	SU01	89.82	69.82	88.76
S6	ASU01	SU01	89.82	69.82	88.76
S8	ASU01	SU01	90.57	70.57	89.51
S9	A11	J080	92.72	72.72	91.66
S10	A12	J070	93.09	73.09	92.03
S12	A22	J040	92.18	72.18	91.12
S13	A5	J050	91.98	71.98	90.92
S14	ASU01	SU01	89.38	69.38	88.32
S15	ASU01	SU01	90.57	70.57	89.51
S16	A5	J050	91.98	71.98	90.92
S17	ASU01	SU01	89.82	69.82	88.76
S18	A11	J080	92.72	72.72	91.66
S19	ASU01	SU01	89.38	69.38	88.32
S20	A9	J090	91.4	71.4	90.34
S21	ASU01	SU01	92.32	72.32	91.26
S22	ASU01	SU01	90.49	70.49	89.43
S24	A12	J070	93.09	73.09	92.03
S25	A13	J060	95.8	75.8	94.74

4.6.5 Simulation periods

The simulations in this study were performed over a continuous period of 01.01.2017 to 25.02.2022 and are not based on single events. In the absence of recorded historical runoff events for the study area, this method identifies the hydrograph and peak runoff events and helps to assess flood dynamics over the period of simulation.

4.6.6 Model calibration and validation

In the absence of an observed hydrograph, the model was calibrated only based on the continuity error and the runoff coefficient. The model was tuned to reduce continuity error to a value close to zero. Parameters of width and slope for each subcatchment were changed

according to table 5.1. Once the continuity error was reduced to the optimal value, the model was used for the runoff coefficient test.

The runoff coefficient was calculated manually for each subcatchment. The runoff coefficient for each type of land use was obtained from the runoff coefficient fact sheet by California Water Board (State Water Resources Control Board, 2009). The average runoff coefficient of each subcatchment was calculated based on the area of different land-use types within each subcatchment. Then the runoff coefficients of subcatchments were compared to manually calculated runoff coefficients.

For model validation, photos from three water accumulated locations in the garden related to the precipitation event on 2nd October 2021 and the map from NIVA's online survey in 2018 indicating water accumulated spots were used. The water accumulation locations from the model were compared to actual water accumulation locations.

The calibrated and tested model was then used for analyzing the results and sensitivity study.

4.6.7 Sensitivity analysis

Sensitivity analysis was performed for the parameters of Manning's roughness for overland flow, soil hydraulic conductivity, bedrock depth, and ground water level to examine how these parameters affect outputs, including peak discharge and water depth.

Manning's roughness number

The model was run for 6 sets of values of manning's n, ±10, ±20, and ±30 % change from the initial value. As explained in section 4.6.1, the initial set of values was estimated based on the suggested table by Rossman (2015).

Hydraulic conductivity

Due to uncertainty about the type of soil and its infiltration rate, four scenarios of soil type and associated hydraulic conductivity were considered in this study, as shown in table 4-8.

Table 4.8: Four scenarios of soil type and associated hydraulic conductivity

Scenario	Low infiltrated soil		Medium infiltrated soil	High infiltrated soil
Soil type	Clay (initial model)	Clay and Anthropogenic **	Anthropogenic and silty loam	Sandy loam
Hydraulic conductivity, Ks*[mm/h]	0.254	1.97	5.1	10.92

* The values are according to Rossman (2015) and Rawls et al. (1983).

** the value of anthropogenic material K_s is from the study by Sæten (2021).

The reason for selecting the first scenario (initial value) is that the area is classified as "low infiltrated" on the infiltration potential map from geonorge.no. The second scenario was selected based on the research conducted in an area close to the current study site (to the west of the allotment), and boreholes in that area show the presence of anthropogenic material (Sæten, 2021). Some locations within the allotment were also filled with anthropogenic material; however, there is no information on the precise locations, extent, depth, or type of this material (Personal communication with co-supervisor/NIVA). The third scenario is based on the same study (Sæten, 2021) that discovered thin layers of silt in several locations of her study site close to the current study area. The fourth scenario was chosen to test the outcomes in the presence of high permeable soil in the area.

Bedrock elevation

Three scenarios of bedrock elevation were chosen for this project based on the boreholes map from genorge.no. The range of bedrock depth was between 0 and 40 m for Oslo. Therefore, the average depth of 20m was chosen as bedrock depth for the initial scenario of bedrock elevation. The second scenario was the minimum depth of 5m. This scenario selection is because there was no bedrock physically observed at the site and due to the presence of garden and possibility of anthropogenic material, the bedrock depth value was chosen 5 m instead of 0 m. The third scenario is based on the maximum depth of the bedrock, which is 40m.

Groundwater level

A high groundwater level scenario with a depth of 30cm was investigated to determine the impact of high groundwater levels on water accumulation in the research area.

4.7 Flood extent map

Based on the water depth in junctions obtained from the SWMM model after simulation and following the geometry of each conduit and the contour lines between two sequent junctions in QGIS, the extent of water inundation was estimated. The map was drawn as a polygon layer in QGIS and then was overlaid on the hybrid google maps for better visualization.

5 Results

5.1 Calibration, continuity error, and validation

Table 5.1 shows how adjusting the parameters of width and slope in the calibration process altered the continuity error. The hydraulic continuity error of the model was reduced from 2.17% to 1.96% after calibration. The final calibrated model is a combination of a 30% increase in the initial value of the width parameter and a 10% increase in the initial value of the slope parameter for each subcatchment.

Table 5.1: Changes in the width and slope parameters during the calibration based on the continuity error

Parameter	Initial value	Variation range	Optimal value	Initial continuity error of the model	Optimal continuity error of the model
Width	Table 4.3	±10, ±20, ±30%	+30%	2.17	1.98
Slope	Table 4.3	±10, ±20, ±30%	+10%	2.17	2.04

A linear regression model was used to compare the model's runoff coefficients to the manually calculated runoff coefficients. Figure 5.1 shows that the SWMM model's runoff coefficient values for subcatchments are close to those calculated manually. Subactchemnt22 had the largest variation of 10% (10% decrease in the model compared to manually calculated value), and the variation on average was 3%. The values of runoff coefficients from the model and manually calculated ones and their variation are shown in table A.3 for all subcatchments.

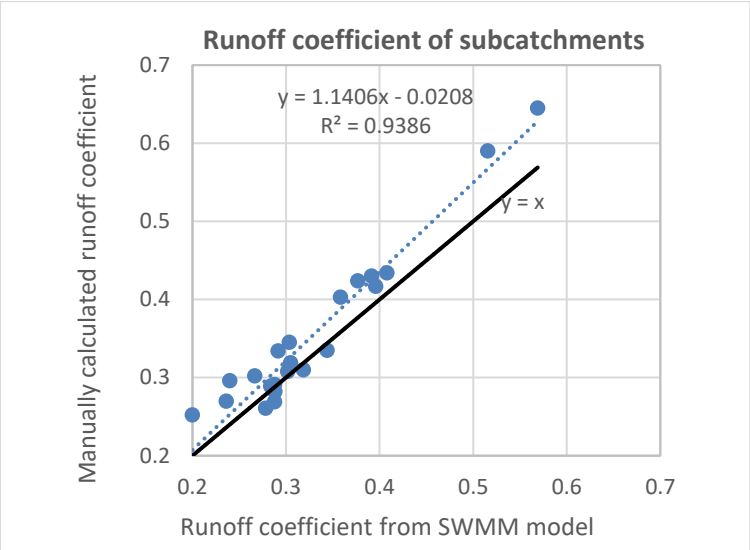

Figure 5-1: Comparison of SWMM model runoff coefficients with manually estimated runoff coefficients using the linear regression model. Blue dots represent subcatchment runoff coefficients. The black line represents a 1:1 linear graph where y=x.

The model was validated using three photos of water accumulation within the allotment related to the 2nd of October 2021 precipitation event. Two photos (figure 5-2, (1 and 2)) taken from the parking lot, west of the allotment, where junctions J030 and J022 of the model are located, show a few centimeters of water depth. The third photo (figure 5-2, (3)) is from a location to the south of the parking lot, where junction J050 of the model is located. The model results showed water accumulation in the same locations as in the photos for the same date. The model reported a maximum water depth of 15, 5, and 9 cm for the deepest part of the junctions J030, J022, and J050, respectively, for the same precipitation event on the 2nd of October 2021. Utilizing images to evaluate the model in terms of the inundation location could be feasible. However, the photos cannot be used as an accurate reference for water depth and demand proper measurement.

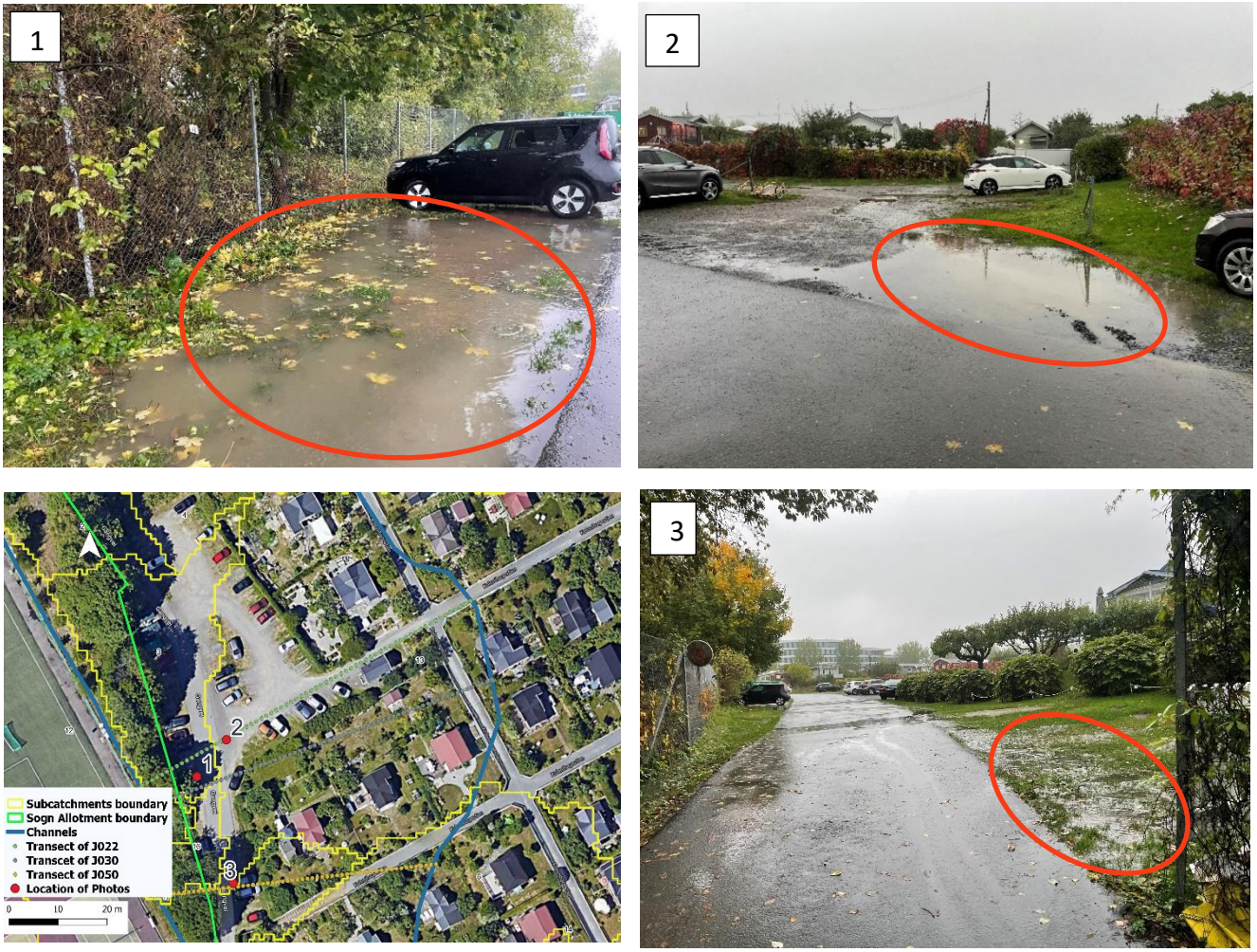

Figure 5-2: Water accumulation related to the precipitation event of 2nd October 2021 in the parking lot in the west of the allotment (Photo no.1, 2, and 3: locations across junction J030, J022, and J050, respectively).The photos were taken by L. J. Barkved/NIVA. The map (bottom, left) was made in QGIS and shows the locations in the garden where photos were taken, the background map is from google maps.

Similarly, water inundation from the model's nodes within the allotment boundary was compared with the water accumulated spots identified by the allotment residents from NIVA's study (see figure 3-3). The inundated locations in the west, southwest and east of the garden generated by the model are in line with the spots in the same locations the residents had been marked on the map. The remaining points from the map 3-3 could not be compared to the model's inundated locations since these points were not in the routing part of the model (inside the channel border). However, at these points, according to the historical recall of the survey's participants, water depth was not observed to be greater than 8 or 9 cm (NIVA, 2018). In addition, by visiting the condition of the terrain, these spots were not identified as problematic

areas. Instead, the channels, as explained in section 4.3, were considered locations of interest in terms of water inundation. There was no similar study for the adjacent areas to compare the real inundated locations to the inundated locations from the model.

5.2 Time series of precipitation, runoff, and water depth

Figure 5-3 shows the time series of precipitation, runoff, and maximum water depth in the storage unit node over the period of simulation.

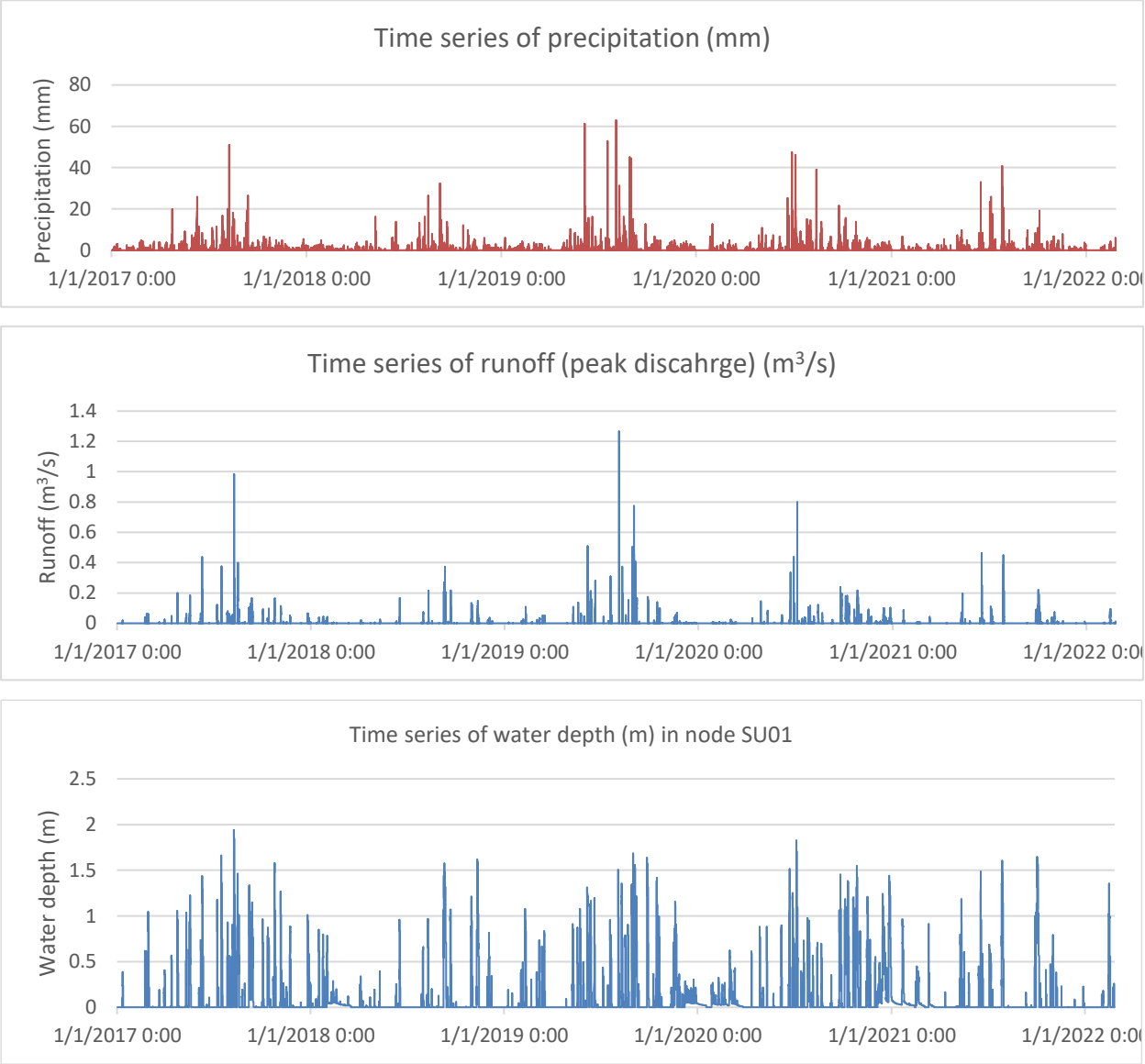

Figure 5-3: Time series of precipitation, runoff, and water depth over the period of simulation

Tables 5.2 and 5.3 show the three highest precipitation events and peak runoff (discharge) of the study area over the period of simulation.

Table 5.2: Three highest precipitation events over the period of simulation

Rank	Start Date	Event Duration (hours)	Event Peak (mm/h)	Return Period (years)
1	04.08.2019	0.7	63	6
2	06.06.2019	22	61.2	3
3	19.07.2019	11.5	52.8	2

Table 5.3: Three highest discharge peak events over the period of simulation

Rank	Start Date	Event Duration (hours)	Event Peak (m3/s)	Return Period (years)
1	04.08.2019	5.7	1.266	6
2	09.08.2017	22.5	0.983	3
3	05.07.2020	13.8	0.8	2

The Storage Unit, which encompasses areas in the west, southwest, and south of the allotment, as shown in figure 4-7, has the highest water depth of 1.94 m in the deepest part. Therefore, the locations within the storage unit are considered critical locations in terms of flood inundation. The maximum water depth in the storage unit occurred on 9 August 2017 (figure 5.4), associated with a peak discharge of 0.983 m3/s. However, the highest peak discharge over the period of the simulation was 1.266 m3/s on 4 August 2019. Therefore, the maximum water depth event did not happen on the same date when the highest peak discharge happened. The difference in date might be rooted in the soil condition, the groundwater condition, and the amount of accumulated water before a particular precipitation event rather than only the amount of precipitation that can affect the water depth.

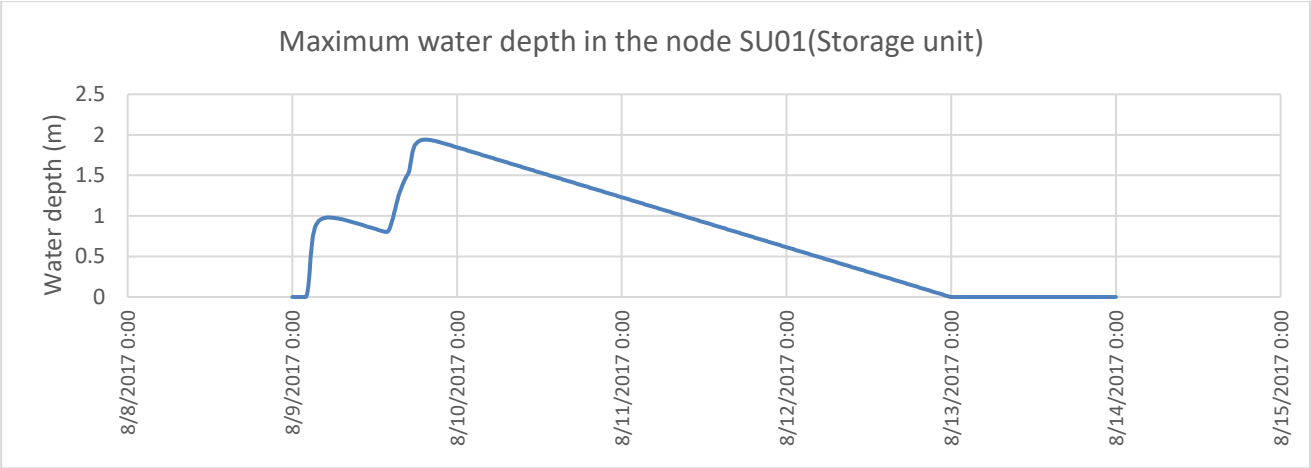

Figure 5-4: Maximum water depth in the node SU01 associated with a peak discharge of 0.983 m3/s on 9 August 2017

Figure 5-5 shows the number of days on which the inundation occurred in the storage unit over the period of simulation. The water level exceeded 1.5 m on 21 occasions over the 1882-day simulation period. However, for 335 of the 1882 days, the water level was less than 20 cm. The maximum and average water depth for all nodes are presented in table A.4.

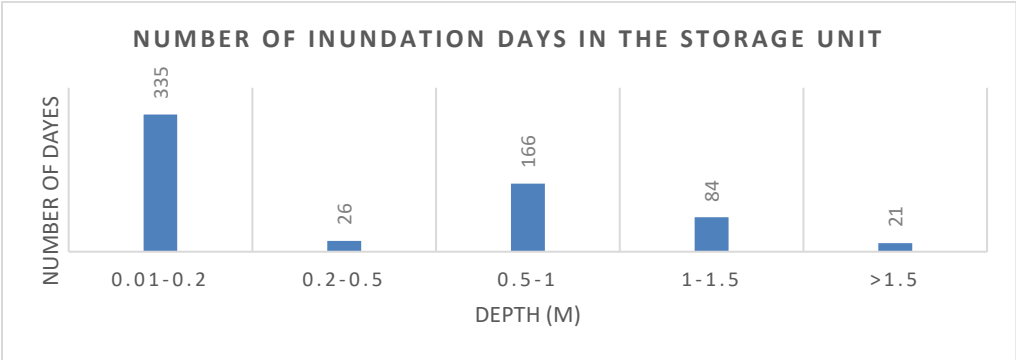

Figure 5-5: shows the number of days on which the inundation occurred in the storage unit over the period of simulation

5.3 Sensitivity analysis

Manning's roughness

The peak discharge from the subcatchments for ±10 %, ±20 %, and ±30% change in the manning' s n of pervious and impervious subareas were compared to the subcatchments peak discharge

associated with the initial value of n (figure 5-6). The peak discharge from subcatchmets showed the highest average variation of 17% and 13% for -30% and +30% change in n value, respectively. Among subcatchments, the highest variation was from subcatchment9, where for 30% decrease in the initial value of n, the peak discharge increased from 0.06 m3/s to 0.08 m3/s (33% variation). The total peak discharge for the whole area changed from 1.26 m3/s to 1.09 m3/s and 1.48 m3/s for 30% increase and 30% decrease in the initial value of n, respectively.

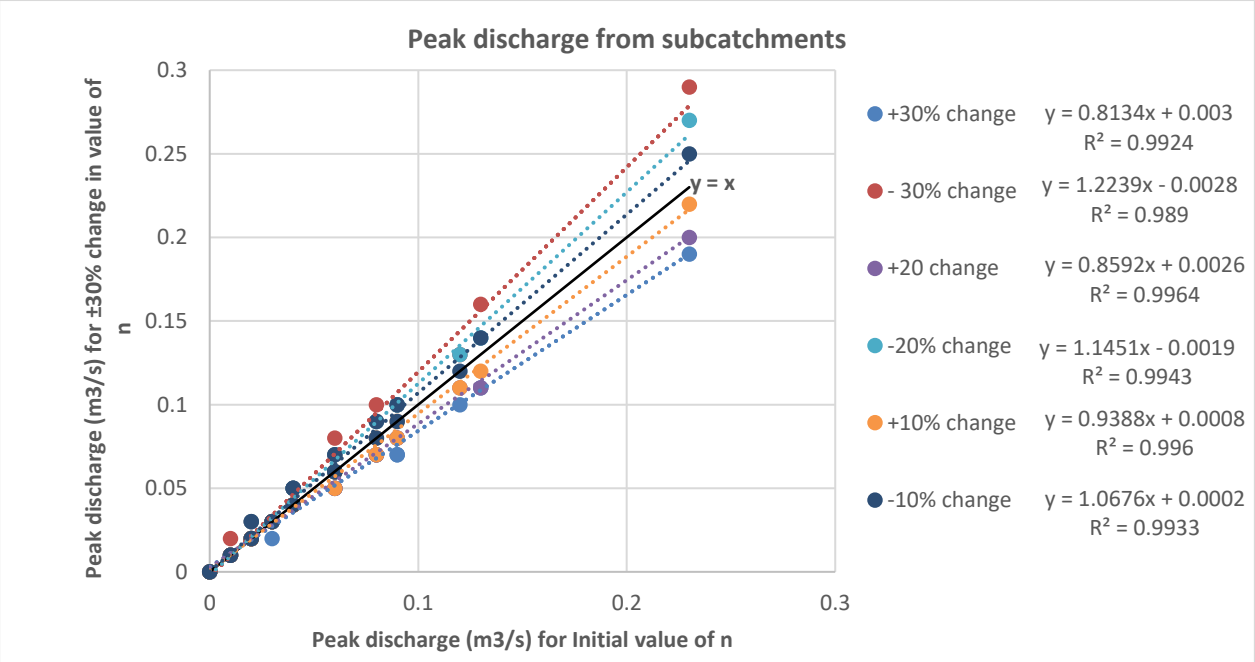

Figure 5-6: Comparison of peak discharge from subcatchments associated with ± 30% change in initial values of n to peak discharges associated with initial values of n using linear regression

However, the changes in maximum water depth in the nodes were not considerable. The maximum water depth in the node SU01 (the critical node) was compared for the range between -30% and +30% change in the initial value of n in figure A.1. The results show that the water depth in the storage unit has a variation of only 2 cm when the n value is changing between +30% and -30% of the initial value.

Hydraulic conductivity

Comparing the simulated peak discharge from the three scenarios of the low, medium, and high infiltrated soil (table 4.8) with the peak discharges associated with the initial soil type of clay showed a decrease in peak discharge in subcatchments illustrated in figure 5-7. Therefore, as

hydraulic conductivity increased, the peak discharge decreased. When hydraulic conductivity increases, a greater fraction of precipitation infiltrates to the ground, and in contrast, a smaller fraction is converted to runoff (runoff ration). The highest decrease belongs to subcatchment 25, where the discharge decreased from 0.09 to 0.01 m3/s as hydraulic conductivity increased from 0.254 to 10.92 mm/h.

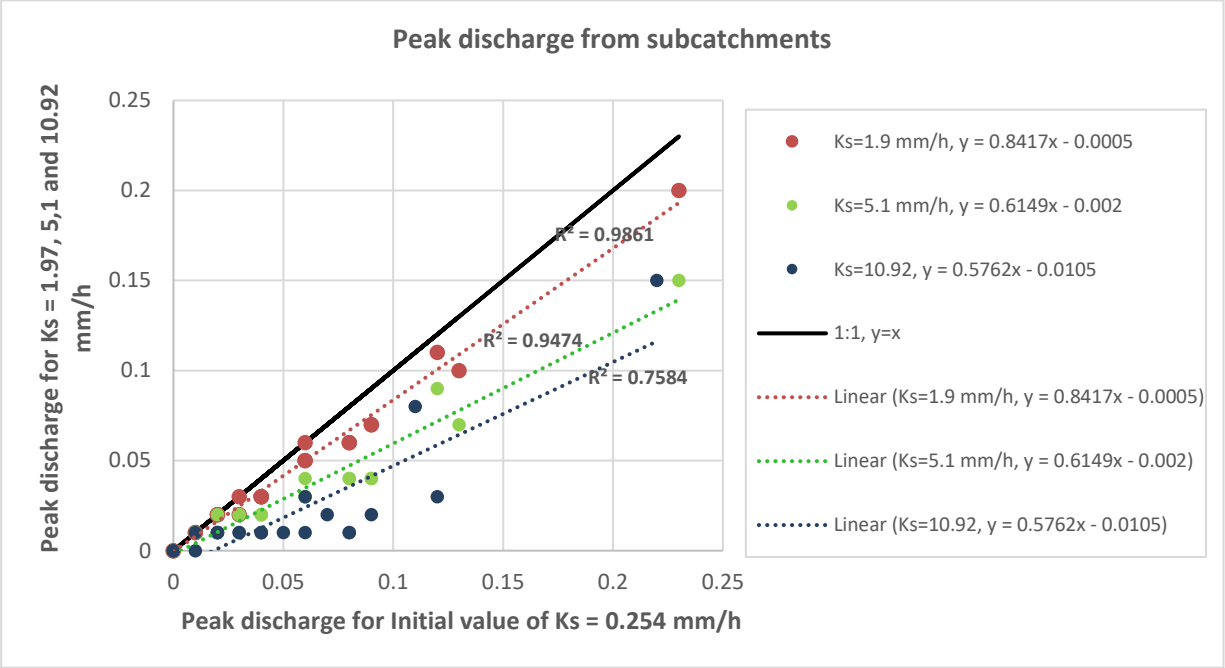

Figure 5-7: Linear regression model of three scenarios of hydraulic conductivity. Dots with three different colors show the simulated peak discharge of subcatchments for each scenario of modified Ks against the simulated peak discharge of subcatchments for the initial value of Ks. The black line is a 1:1 graph with the value of y=x.

Table 5.4 shows the peak discharge from the whole study area for different scenarios of hydraulic conductivity as well as for the initial value. The peak discharge of the whole area decreased 71%, from 1.266 m3/s for the initial scenario with ks=0.254 mm/h to 0.363 m3/s for the scenario with ks=10.92 mm/h.

Table 5.4: Simulated peak discharge of the whole study area from four scenarios of hydraulic conductivity

Hydraulic conductivity, Ks (mm/h)	0.254	1.97	5.1	10.92
Peak discharge (m^3/s)	1.266	1.031	0.666	0.363

The maximum water depth in the nodes decreased by increasing the hydraulic conductivity. The storage unit had the largest drop in maximum water depth. The maximum water depth for the storage unit was reduced from 1.94 m to 1.67, 1.47, and 1.46 m for the scenarios of Ks=1.9, Ks=5.1, and Ks=10.92 mm/h, respectively. The date of the maximum depth event changed from 09.08.2017 to 24.09.2020 when Ks changed from 1.97 to 5.1 mm/h. Maximum water depth in two models with Ks of 5.1 and 10.92 happened on the same date (24.09.2020).

Bedrock depth

The two scenarios of bedrock elevation (min and max) only affected the simulated groundwater level from subcatchments over the period of simulation (Figure A-2), but not the peak runoff from the subcatchments and the depth of water in the nodes. The range of variation in groundwater level is between 0 and 6 cm for both scenarios at subcatchment17's outlet (associated with the deepest part of the storage unit).

5.4 Runoff estimation by source

The generated runoff, infiltration, and evaporation (water budget components) by source (within the garden vs. outside the garden) in mm and percentage over the period of simulation are presented in figures 5-8 and 5-9.

As figures 5-8 and 5-9 show, the generated runoff is less from the garden than from adjacent areas, 1266 mm vs. 1807 mm (29% vs. 42% of total precipitation). In other words, the fraction of precipitation into the runoff (runoff ratio) is less from the garden than outside the garden (0.29 vs. 0.42). This difference is because the subcatchments outside the garden included more impervious surfaces than those within the garden. The generated runoff from each subcatchment with specifying subcatchment location in the study site is provided in table 5.5.

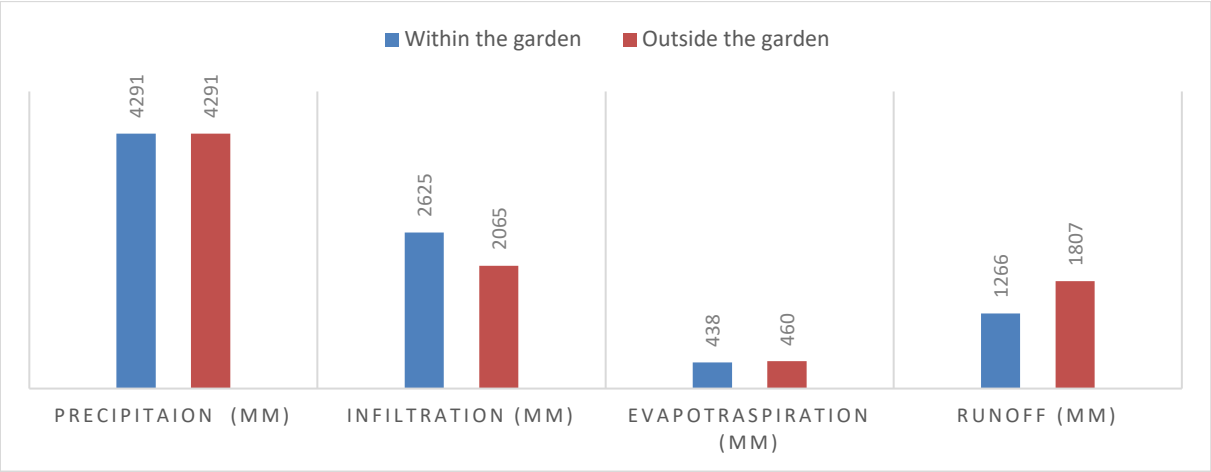

Figure 5-8: Comparison of the generated runoff, infiltration, and evaporation (in mm) between inside and outside the garden in response to the precipitation of 4291mm over the period of simulation

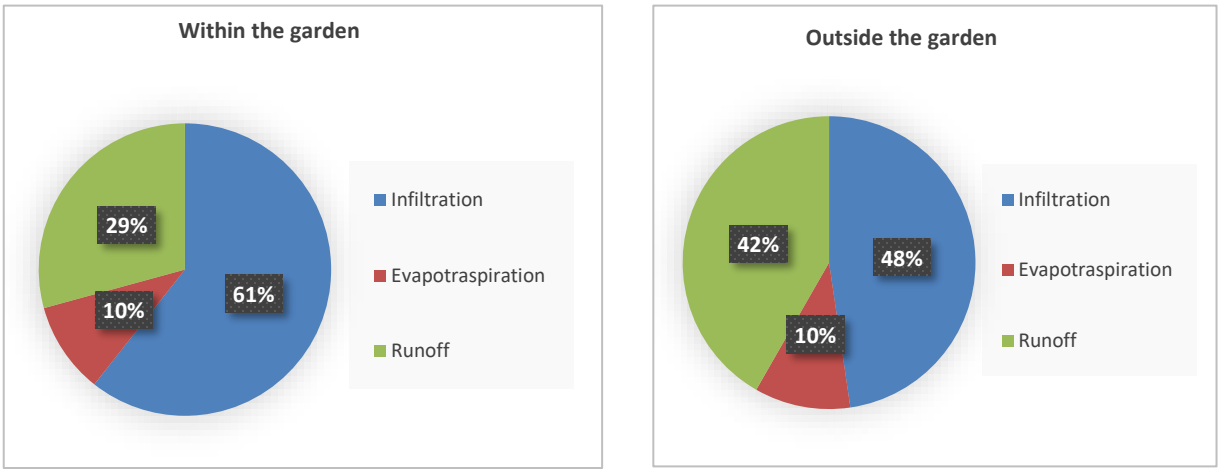

Figure 5-9: Comparison of the generated runoff, infiltration, and evaporation (in percentage) between inside and outside the garden in response to the precipitation of 4291mm over the period of simulation

Table 5.5 shows the peak discharge for different subcatchments with specifying the location of each subcatchment within the study area. The comparison of the peak runoff discharges from subcatchments shows that the highest peak discharge with the value of 0.23 m3/s belongs to subcatchment 8, which is located outside the garden boundary. The second and third highest peak discharges, 0.13 and 0.12 m3/s, belong to subcatchment 15 and 5, respectively. Subcatchment 15 is located partially inside and partially outside the garden. Subcatchment 5 is outside the garden.

Table 5.5: peak discharge from subcatchments and the location of each subcatchment in the study area (within and outside the garden or with a shared area in both).

Subcatchment ID	Location of the subcatchment in the study area	Peak discharge (m3/s) (highest to lowest)	Runoff (mm)
S8	Outside the garden	0.23	1843.91
S15	Both	0.13	1438.48
S5	Outside the garden	0.12	2531.8
S13	within the garden	0.09	1241
S25	within the garden	0.09	1211.43
S4	within the garden	0.08	1249.51
S24	Both	0.08	1323.28
S1	within the garden	0.06	1120.47
S9	Both	0.06	1155.72
S20	Both	0.06	1787.8
S14	within the garden	0.04	1160.17
S2	Both	0.04	1080.59
S12	Both	0.04	1330.98
S10	Outside the garden	0.03	1863.38
S21	Both	0.03	1432.62
S6	within the garden	0.02	1370.27
S17	Both	0.02	1271
S19	Both	0.02	1480.64
S3	Both	0.01	1297
S22	Both	0.01	2769.39
S18	Outside the garden	0	1729.75
S16	Both	0	1821.11

The peak discharge values from sucatchments inside the garden were added up to estimate the total peak runoff within the garden. Similarly, the peak discharge for the outside of the garden was estimated. The peak discharge for those subcatchments with the shared area between inside and outside the garden is distributed based on the area inside and the area outside the garden. The peak discharge contribution by sources is shown in figure 5.10 in m3/s and in percentage.

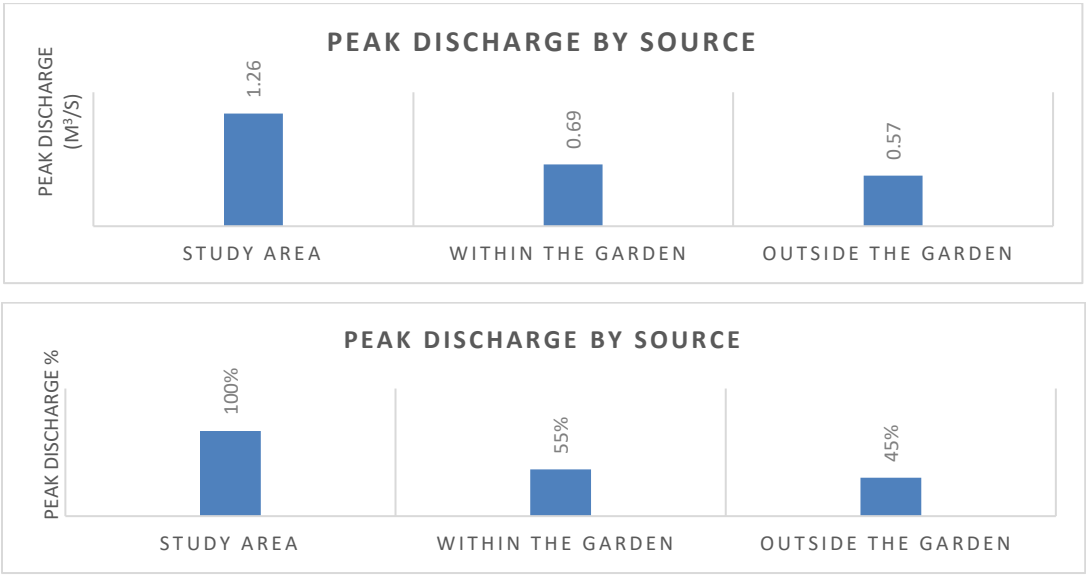

Figure 5-10: The peak discharge of 1.26 m3/s (4/8/2019) by its generation source. The top graph shows the discharge value in m3/s, and the bottom graph shows the percentage of the discharge.

The share of the garden from the total peak discharge is larger than the share of the outside of the garden (55% vs.45%). This is due to the larger area (60% of the total study area) for the inside garden than for the outside (40%). However, peak discharge in relation to the area is less for the area inside than for the outside (0.08 vs. 0. 09 m3/s/ha).

5.5 Flood inundation maps

The flood inundation maps (figure 5-11) show the maximum extent and depth of inundation over the simulation period. The greatest maximum extent and depth of inundation in the area belongs to the storage unit (node SU01) which was associated with the peak runoff of 0.983 m3/s on 9 August 2017. The second highest depth, with the value of 24 cm, belongs to the nodes J030 and J040, both located in the south of the parking area (figure 5-13, orange circle). The second highest depth was associated with the peak runoff of 1.26 m3/s on 4 August 2019. The maximum inundation depth in the remaining locations of flood inundation maps (figure 5-11) was under 20 cm. The maximum inundation depth of all nodes is represented in table A.4.

Infrastructure locations are the most vulnerable locations to flood inundation. As shown in figure 5-12, five cabins in the storage unit location, four in the west of the garden and one in the south, are at the risk of flooding. Furthermore, two asphalt roads in the storage unit, one to the west of the garden and the other to the south, can be damaged by the water inundation. The maximum water depth was 1.94 m in the storage unit's deepest part, right adjacent to the inundated cabins (figure 5-12, bottom). The highest water inundated level in the four cabins in the west was 1.5 meters from the ground surface in their positions (The cabins are elevated from the ground surface by about half a meter). For the cabin located in the south, the maximum water inundated level is 70 cm from the ground surface, including the cabin's base, which is elevated about half a meter.

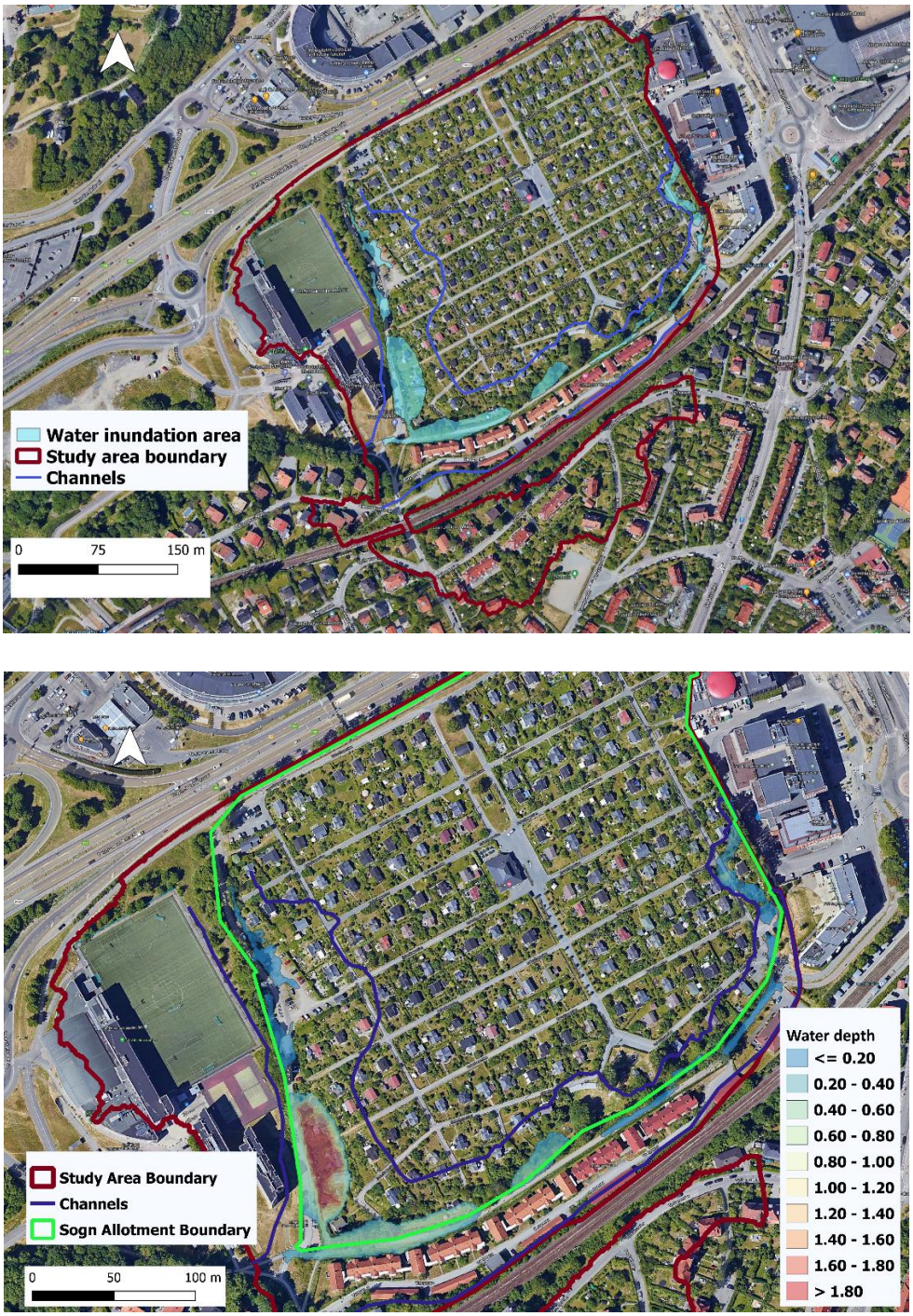

Figure 5-11: Maximum flood inundation maps, showing the maximum extent (top) and the depth of inundation in the study area over the period of simulation. The maps were made in QGIS. The background map is from Google maps.

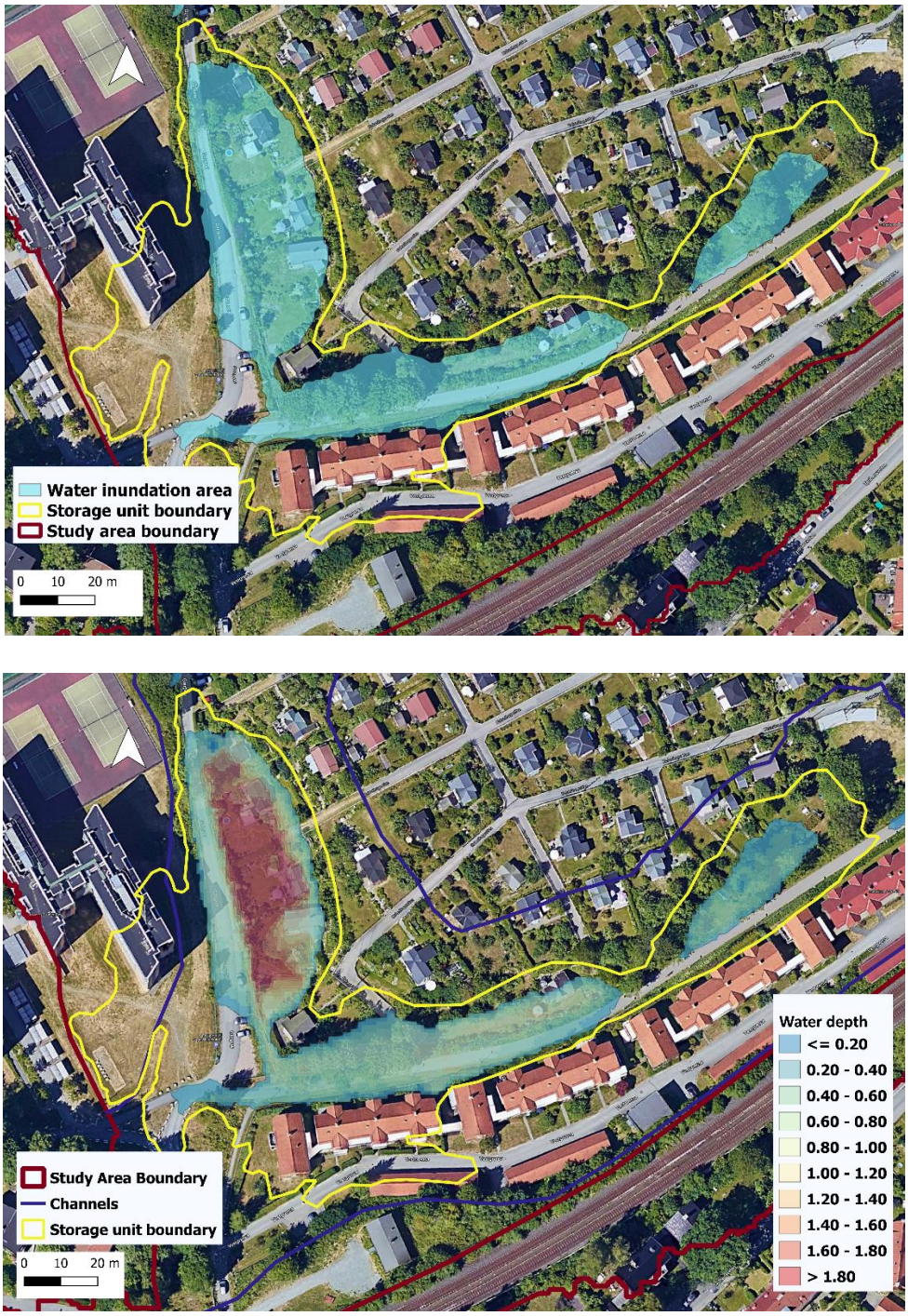

Figure 5-12: Maximum flood extent (top) and flood depth map (bottom) in the storage unit (node) SU01, showing the extent of inundation in the storage unit (node SU01). The map was made in QGIS. The background map is from Google maps.

Figure 5-13: Maximum flood extent and depth in the parking area (west of the allotment garden). The highest water depth for this area was 24 cm in the south of the parking lot (orange circle). The map was made in QGIS. The background map is from Google maps.

Runoff in the study area flew towards the channels and within the channels mainly accumulated in the storage unit, which is situated in depression. By considering the garden's boundary (figure 5.11 bottom), the inundated locations were mainly situated within the garden (77% of the whole inundated area). However, as discussed before, the source of the runoff that caused the inundation is mainly the area outside the garden (29% runoff from the garden vs. 42% from outside the garden).

6 Discussion

The results of the model and further analysis of the model results revealed the sources of runoff in the research area, the flood inundation extent, and depth. The results can be affected by the input data and method. Due to the lack of measured input data and boundary conditions such as hydraulic conductivity, bedrock depth and … , some assumptions were made in this study. Therefore, there are several sources of uncertainty associated with the assumptions data as well as the method applied. In this section, the sources of uncertainty, as well as implications of the results, will be discussed.

6.1 Input data and boundary condition

Hydraulic conductivity

When establishing a water budget, the infiltration capacity and hence hydraulic conductivity are critical . The saturated hydraulic conductivity scenarios of this study showed a large variation in results. The heterogeneity of the soil in Oslo causes substantial differences within small regions, as evidenced by Bjørvik (2021) through fieldwork using the Mariotte device in the Gaustad catchment (Bjørvik, 2021). While in the current study, the hydraulic conductivity value was the same for all subcatchmets in the absence of measured infiltration data. In addition, there are a few publications documenting Oslo's infiltration capacity, and the map depicting the infiltration potential from NGU contains inherent weaknesses. The polygon boundaries reflecting the various degrees of infiltration potential are clearly drawn from geological mapping and follow the soil sediment maps from NGU rather than measuring the infiltration rate (Bjørvik, 2021). The map does not show the actual infiltration rate but rather an indicator of infiltration potential. As explained before, the Sogn allotment garden was categorized as “not suited” for infiltration. Using this map as an input is not very practical because it may generate misleading results.

The saturated hydraulic conductivity of clay was chosen 0.254 mm/h from Rossman & Huber (Rossman & Huber, 2016, p. 114). However, according to Dingman (2015), the saturated hydraulic conductivity for clay is 10^{-11} to 10^{-7} mm/h (Dingman, 2015, p. 325). This can cause a significant variation in the results. Nevertheless, on the other hand, choosing a lower value of hydraulic conductivity than the current one might not be a reasonable choice since it leads to a

greater water depth, as shown from the sensitivity analysis results. The water depth associated with the 2nd October 2021 precipitation event in the model with the current hydraulic conductivity of 0.254 mm/h showed similarity with the actual condition of water accumulation on the west side of the garden.

Furthermore, based on historical recall of the residents of the allotment, the water did not go up more than around half a meter in the deepest part of the storage unit so far (Personal communication with co-supervisor/NIVA). While with the current value of hydraulic conductivity of 0.254, the simulated maximum water depth in the storage unit showed overestimation. Therefore, if the hydraulic conductivity decreases to a value less than the current one, for instance, the value of 10^{-11} to 10^{-7} mm/h suggested by Dingman (Dingman, 2015, p. 325), it leads to even more overestimation.

In urban environments, hydraulic conductivity often declines with depth (Sari, 2022). Therefore, the model with a saturated hydraulic conductivity of 0.254 mm/h without considering soil depth may not be realistic.

Groundwater elevation

For all aquifers in this study, the value of initial groundwater levels was estimated based on the average groundwater depth. The average groundwater depth with the value of 1.06 m, as explained in section 4.6.4, was estimated from the data recorded by the three loggers in subcatchment9. Two of these three loggers were so close to each other, both in the center of the subcatchment, and the third close to the subcatchment's outlet. However, due to uncertainty in the type of soil and bedrock depth at different locations within the research area, groundwater depth may vary for different subcatchments in reality. Yet, on the other hand, in the lack of measured groundwater depth from various locations within the study area, it sounds logical that groundwater levels be estimated by following the topography. Furthermore, according to Beldring (2020), groundwater in Scandinavia often follows topography (Beldring, 2002).

On the other hand, there was another source of uncertainty with the period of recorded groundwater data. The loggers recorded groundwater levels from 18.12.2021 to 30.03.2022,

while the beginning of the simulation period was 01.01.2017. The average groundwater depth from this period may not represent the real groundwater depth at the beginning of the simulation period. However, the recorded data is from the same season as the beginning of the simulation period, which can reduce the uncertainty.

For assessing the effect of the initial groundwater level, a scenario of a low groundwater depth of 30cm was simulated as well. However, this only affected the simulated groundwater level from subcatchment over the period of simulation but not the peak runoff from the subcatchments and the depth of water in the nodes.

Manning's n for overland flow

Manning's n for pervious and impervious subareas is an essential input parameter in the coupled hydrological-hydraulic models, determining bottom roughness in overland flow (Sanz-Ramos et al., 2021). The sensitivity analysis in this study showed that by decreasing the value of Manning's n, the peak discharge increased and vice versa. This is because the value of n, contributing to the material roughness and sub-area geometric elements, affects friction or energy loss. The friction of the surface has an effect on the speed of the overland flow and hence the time of concentration and peak flow (Sanz-Ramos et al., 2021). However, according to the sensitivity analysis, changing the Manning's n had a negligible effect on water depth in the storage unit. This is due to the terrain condition of the storage unit, which is in depression, resulting in water accumulation instead of flowing out of the depression. As a result, friction and, therefore, the n value is ineffective factors on water depth in the storage unit, whereas infiltration characteristics such as hydraulic conductivity, which influences infiltration rate, as described previously, are effective parameters on water depth.

6.2 Continuity error, calibration, and validation

Calibration of a model is important to assure the model's quality. Typically, the observed values are compared to the model-generated values in a calibration process. Due to a lack of observed data, such as water depth and discharge, the model was calibrated against continuity error and runoff coefficient by changing the parameters of width and slope. This comparison might not be a proper method since the simulated values such as discharge and water depth cannot be

compared to a reference outside the model. However, using historical data in the calibration process does not necessarily provide a reliable model in SWMM due to possible bias in input data and model parameters (Xichao et al., 2020).

Continuity error

As described in section 2.4.8, a higher value of continuity error indicates a greater imbalance in the water budget. The preliminary model, as explained in section 4.6.2, showed a large continuity error of -350 %. This was mainly due to the conduits' adverse (negative) slopes located in the depression areas (southwest and south of the allotment). The routing method in that model was dynamic wave, which was supposed to solve the routing equation even under adverse slope conditions. However, the high error demonstrated that the dynamic wave routing method is not a good choice in open channel conduits under adverse slope circumstances. The second/current model was created to reduce the continuity error. The conduits with adverse slopes were removed, and the subcatchments that drained to the depression junctions were then drained to the storage unit. Due to removing adverse slopes, the kinematic wave was used as the routing method. The continuity error dropped to - 2.17 %, and the running time from about 10 min dropped to around 1min.

The model with the storage unit and the continuity error of -2.17% was used for calibration. The model was tuned by modifying the width and slope parameters to reduce continuity error. The calibrated model's continuity error was reduced to -1.95 %. However, calibrating a model that is already within an acceptable range of continuity error (less than 5%) to reduce continuity error (preferably to zero) may not result in a more reliable model. This is because changing the width and slope parameters affects the outcomes, including peak discharge and maximum water depth, and may make the results implausible (overestimated or underestimated). Due to a lack of observed data to compare, the reliability of results cannot be judged properly in this aspect.

Runoff coefficient

The comparison of the runoff coefficients calculated manually and from the model revealed insignificant differences (Table A.3). The comparison indicated that the calibrated model produced acceptable runoff coefficient results. However, this comparison may not be precise

enough because the manually calculated runoff coefficients could have different values when referring to different sources. Rather than only land type, the runoff coefficient is modified by a range of components and conditions, including slope and rainfall severity. As a result, there are differences in values between different references. For instance, the runoff coefficient for the garden was estimated as the average value of agricultural land with heavy soil and woodland based on a fact sheet from the United States Water Resources Control Board (State Water Resources Control Board, 2009), which resulted in a value of 0.20. While Li et al. (2014). suggested a value of 0.1 (Li et al., 2014). Despite the explained uncertainty, this comparison of the runoff coefficient could be an acceptable criterion for adjusting the model due to the absence of observed data for calibration.

Validation

In terms of model validation, referring to the photos of water accumulation related to the precipitation event of 2nd October 2021, which were taken from almost the same location, is insufficient. Although the model showed similarities with the photos in terms of location and depth of accumulated water in the west of the allotment, this does not necessarily mean that the other locations would show similarities in this regard. The reason for that could be the possibility of soil variation within the study area, resulting in a difference between the model's results and reality for some locations and similarity for others. In other words, the type of soil and associated parameters such as hydraulic conductivity for one subcatchment may differ from the other, resulting in differences in outputs. While, due to a lack of measured infiltration data, all subcatchments in the model were assigned the same hydraulic conductivity value based on the infiltration potential map.

6.3 Method and results

Water budget within and outside the allotment garden

As shown in figures 5-8 and 5-9, the water budget results revealed a significant difference between the areas within the allotment garden and the areas outside the garden. The water budget for the allotment garden indicated 61% infiltration, 10% evaporation, and 29% runoff, whereas, for the outside of the garden, 42% infiltration, 10% evaporation, and 48% runoff were

estimated. Therefore, the nearby regions of the garden with more impervious surfaces, such as asphalt roads and buildings, generated more runoff than the garden. The positive impact of impervious surfaces on runoff is supported by Bjørvik (Bjørvik, 2021), which found that urbanization in the Gaustad catchment has resulted in higher runoff when comparing natural and urban subcatchments within the Gaustad catchment. Furthermore, the water budget results are consistent with earlier studies on the hydrological effects of impermeable surfaces on infiltration, evaporation, and surface runoff (Dupont et al., 2006; Fletcher et al., 2013; Schirmer et al., 2012). These studies showed a positive correlation between urbanization and an increase in runoff as well as a decrease in infiltration.

However, there is uncertainty in the method used to calculate the water budget by source in this study. This uncertainty relates to the subcatchmets with the shared area inside and outside the garden. The SWMM model only provides the water budget components for the entire subcatchment. As a result, for those subcatchments with the shared area, the value of infiltration, evaporation, and runoff from the model was divided in relation to the share of the area of a subcatchment within and outside the garden. However, this may be inaccurate because characteristics such as slope, pervious and impervious subareas may differ from one side of a subcatchment to the other side. These differences were not considered in the allocation of runoff and other water budget components, resulting in inaccurate outputs and mapping of the extent of water.

Flood maps and inundation extent

As flood maps showed, the inundated locations were mainly within the garden. Of the total inundated area, 77% was within the garden, and 23% was outside the garden; however, as discussed before, the source of the runoff leading to inundation is mainly outside the garden (29% runoff from the garden vs. 42% from outside the garden). This shows the role of the garden in flood retention due to its terrain condition and the presence of the areas in depression within the boundary of the garden beside the main role of the garden in the infiltration of surface runoff (61% infiltration within the garden vs. 48% outside the garden).

The flood extent was mapped based on the maximum water level in the nodes. In SWMM, only one transect can be allocated between two nodes, and the geometry of the conduit is considered the same along the conduit between two nodes. Therefore, the terrain condition between two nodes is ignored, resulting in inaccuracies while mapping the inundated extent.

Continuous simulation

Time series results of the model showed the maximum water depth over the period of simulation in the critical locations was not necessarily associated with the highest peak discharge and the most critical precipitation event. Therefore, the continuous stimulation may provide more accurate water depth results than the single event simulation and therefore aids in generating more accurate water inundation maps. According to Hossain et al. (2019), continuous simulation can consider initial circumstances such as initial soil moisture status, stream and reservoir level, and water table level (Hossain et al., 2019). While event-based models are unable to reflect the initial conditions; instead, values are assigned subjectively by the user and calibrated using an observed hydrograph (Green & Stephenson, 1986). As a result, a single event simulation might not necessarily provide the critical water depth and may lead to unrealistic flood inundation maps, especially in the absence of observed data. In addition, Cunderlik and Simonovic (2005), based on a study in an urbanized river basin in southwestern Ontario, Canada, concluded that continuous simulation generated more trustworthy hydrographs (Cunderlik & Simonovic, 2005). On the other hand, other researchers such as Azmat et al, De Silva et al., Hossain et al. showed that the event-based simulation resulted in more accurate results.

7 Conclusion

Estimation of the generated runoff by source revealed that the runoff from the garden is less than from outside the garden (29% vs. 42%). In contrast, the infiltration inside the garden was larger than outside the garden (61% vs. 48%). This is due to the land cover in the allotment garden, which mainly consists of garden and, in general, more pervious land than the adjacent areas.

The inundated area within the boundary of the channels is larger in the garden than outside the garden (77% vs. 33%). This is due to specific terrain conditions at the research site encompassing locations in the depression, mainly within the garden (the location of the storage unit). Therefore, the allotment garden has a considerable role in flood retention in this area.

The critical location associated with the maximum inundation depth of 1.94 m is within the garden, in the deepest part of the storage unit. Five cabins and two asphalt roads in the storage unit were identified as the study area's most vulnerable infrastructures to inundation.

The validation of the model showed similarity in the location of water accumulation in the parking area (western part of the allotment garden) between the photos and the model results for the same precipitation event.

The sensitivity analysis of the parameters of Manning's n for overland flow, hydraulic conductivity, bedrock depth, and groundwater level showed the model is more sensitive to hydraulic conductivity and less sensitive to bedrock depth and groundwater level. Runoff volume, peak runoff, and the nodes' maximum water depth decreased while the hydraulic conductivity increased.

Further work:

i. The infiltration capacity across the study area needs to be measured, and the possible heterogeneity of the soil should be considered for further study.

ii. The possibility of applying different low impact development (LID)/blue-green infrastructure solutions in the subcatchments with high contribution to peak runoff can be investigated. In addition, their impacts on the runoff can be studied through modeling.

iii. Measurement of the accumulated water depth in the storage unit, particularly adjacent to the most critical inundated cabins, to record water level after rainfall events would be beneficial in calibrating the model (possibly using a sensor in the storage unit).

iv. Investigation of the ground condition and possibly borehole excavation to find out the bedrock's depth and map the layers of the soil, particularly the extent and depth of possible anthropogenic material at the study site.

v. Groundwater levels should be measured for more locations across the study area and possibly for longer periods.

References

Adhikari, U. (2020). *Vulnerability assessment of urban flooding in Lerum Municipality and study of effectiveness of blue-green mitigation measures using software MIKE 21 and SCALGO Live [Master's thesis].* University of Chalmers.

Alexander, K., Hettiarachchi, S., Ou, Y., & Sharma, A. (2019). Can integrated green spaces and storage facilities absorb the increased risk of flooding due to climate change in developed urban environments? *Journal of Hydrology*, *579*, 124201.

Barco, J., Wong, K. M., & Stenstrom, M. K. (2008). Automatic calibration of the U.S. EPA SWMM model for a large urban catchment. *Journal of Hydraulic Engineering*, *134*(4), 466-474. https://doi.org/doi:10.1061/(ASCE)0733-9429(2008)134:4(466)

Beldring, S. (2002). Runoff generating processes in boreal forest environments with glacial tills. *Hydrology Research*, *33*(5), 347-372. https://doi.org/10.2166/nh.2002.0013

Bjørvik, F. V. (2021). *Urban impact on water quality and the local water budget-Gaustad [Master's thesis].* University of Oslo.

Bulti, D. T., & Abebe, B. G. (2020). A review of flood modeling methods for urban pluvial flood application. *Modeling Earth Systems and Environment*, *6*(3), 1293-1302. https://doi.org/10.1007/s40808-020-00803-z

Cunderlik, J., & Simonovic, S. (2005). Hydrological extremes in a southwestern Ontario river basin under future climate conditions. *Hydrological Sciences Journal-journal Des Sciences Hydrologiques - HYDROLOG SCI J*, *50*, 1-654. https://doi.org/10.1623/hysj.2005.50.4.631

Dawson, D. A., Vercruysse, K., & Wright, N. (2020). A spatial framework to explore needs and opportunities for interoperable urban flood management. *Philosophical Transactions of the Royal Society A: Mathematical, Physical and Engineering Sciences*, *378*(2168), 20190205. https://doi.org/doi:10.1098/rsta.2019.0205

Dickinson, R. (2002). *Pervious surface roughness values*. Retrieved May 4 from https://www.openswmm.org/Topic/2218/pervious-surface-roughness-values

Dickinson, R. (2010). *SWMM knowledge base*. Retrieved May 15 from https://www.openswmm.org/Topic/4223/interpreting-continuity-error

Dingman, S. L. (2015). *Physical hydrology* (3rd ed.). Waveland Press Inc.

Dupont, S., Mestayer, P., Guilloteau, E., Berthier, E., & Andrieu, H. (2006). Parameterization of the urban water budget with the submesoscale soil model. *Journal of Applied Meteorology and Climatology - J APPL METEOROL CLIMATOL*, *45*, 624-648. https://doi.org/10.1175/JAM2363.1

Endreny, T. (2006). Land use and land cover effects on runoff processes: Urban and suburban development. https://doi.org/10.1002/0470848944.hsa122

Feng, B., Zhang, Y., & Bourke, R. (2021). Urbanization impacts on flood risks based on urban growth data and coupled flood models. *Natural Hazards*, *106*(1), 613-627. https://doi.org/10.1007/s11069-020-04480-0

Fletcher, T. D., Andrieu, H., & Hamel, P. (2013). Understanding, management and modelling of urban hydrology and its consequences for receiving waters: A state of the art. *Advances in Water Resources*, *51*, 261-279. https://doi.org/https://doi.org/10.1016/j.advwatres.2012.09.001

Fletcher, T. D., Shuster, W., Hunt, W. F., Ashley, R., Butler, D., Arthur, S., . . . Viklander, M. (2015). SUDS, LID, BMPs, WSUD and more – The evolution and application of terminology surrounding urban drainage. *Urban Water Journal*, *12*(7), 525-542. https://doi.org/10.1080/1573062X.2014.916314

Geological Survey Of Noway (NGU). *Datasets*. GeologicalSurveyOfNoway. Retrieved May 2 from https://www.ngu.no/en/topic/datasets

Green, D., O'Donnell, E., Johnson, M., Slater, L., Thorne, C., Zheng, S., . . . Boothroyd, R. J. (2021). Green infrastructure: The future of urban flood risk management? *WIREs Water*, *8*(6), e1560. https://doi.org/https://doi.org/10.1002/wat2.1560

Green, I. R. A., & Stephenson, D. (1986). Criteria for comparison of single event models. *Hydrological Sciences Journal*, *31*(3), 395-411. https://doi.org/10.1080/02626668609491056

Guo, K., Guan, M., & Yu, D. (2021). Urban surface water flood modelling – a comprehensive review of current models and future challenges. *Hydrol. Earth Syst. Sci.*, *25*(5), 2843-2860. https://doi.org/10.5194/hess-25-2843-2021

Hossain, S., Hewa, G. A., & Wella-Hewage, S. (2019). A Comparison of continuous and event-Based Rainfall–Runoff (RR) modeling using EPA-SWMM. *Water*, *11*(3), 611.

Huang, Y., Tian, Z., Ke, Q., Liu, J., Irannezhad, M., Fan, D., . . . Sun, L. (2020). Nature-based solutions for urban pluvial flood risk management. *Wiley Interdisciplinary Reviews: Water*, *7*(3), e1421.

Jamali, B., Löwe, R., Bach, P. M., Urich, C., Arnbjerg-Nielsen, K., & Deletic, A. (2018). A rapid urban flood inundation and damage assessment model. *Journal of Hydrology*, *564*, 1085-1098. https://doi.org/https://doi.org/10.1016/j.jhydrol.2018.07.064

Jato-Espino, D., Sillanpää, N., Charlesworth, S. M., & Andrés-Doménech, I. (2016). Coupling GIS with stormwater modeling for the location prioritization and hydrological simulation of permeable pavements in urban catchments. *Water*, *8*(10), 451.

Lamond, J., & Everett, G. (2019). Sustainable Blue-Green Infrastructure: A social practice approach to understanding community preferences and stewardship. *Landscape and Urban Planning*, *191*, 103639. https://doi.org/https://doi.org/10.1016/j.landurbplan.2019.103639

Li, H., Gao, H., Zhou, Y., Xu, C.-Y., Ortega M., R. Z., & Sælthun, N. R. (2020). Usage of SIMWE model to model urban overland flood: a case study in Oslo. *Hydrology Research*, *51*(2), 366-380. https://doi.org/10.2166/nh.2020.068

Li, J., Zhang, B., Li, Y., & Li, H. (2018). Simulation of rain garden effects in an urbanized area based on Mike flood. *Water*, *10*, 860. https://doi.org/10.3390/w10070860

Li, Z., Wu, L., Zhu, W., Hou, M., Yang, Y., & Zheng, J. (2014). A new method for urban storm flood inundation simulation with fine CD-TIN surface. *Water*, *6*, 1151-1171. https://doi.org/10.3390/w6051151

Maghsood, F. F., Moradi, H., Massah Bavani, A. R., Panahi, M., Berndtsson, R., & Hashemi, H. (2019). Climate change impact on flood frequency and source area in northern Iran under CMIP5 Scenarios. *Water*, *11*(2), 273.

Meng, M. (2021). *How to check mass balance/continuity error in XPSWMM/XPSTORM*. Retrieved May16 from https://mel-meng-pe.medium.com/how-to-check-mass-balance-continuity-error-in-xpswmm-xpstorm-49d17345f36

Moheseen, F. A. (2015). *Urban Runoff Drainage: Case of Kjelsrud in Oslo [Master's thesis].* Norwegian University of Life Sciences.

Müller, A., Österlund, H., Marsalek, J., & Viklander, M. (2020). The pollution conveyed by urban runoff: A review of sources. *Science of The Total Environment*, *709*, 136125. https://doi.org/https://doi.org/10.1016/j.scitotenv.2019.136125

NIVA. (2018). *Overvannshåndtering i Sogn Hagekoloni - kartbasert spørreundersøkelse om overvann og blågrønne løsninger* (NIVA-rapport;7236, Issue. N. i. f. vannforskning. http://hdl.handle.net/11250/2486099

Norwegian Center for Climate Services. (2022). *Observations and weather statistics*. Norwegian Center for Climate Services. Retrieved Feb 28 from https://seklima.met.no/

Peel, M. C., Finlayson, B. L., & McMahon, T. A. (2007). Updated world map of the Köppen-Geiger climate classification. *Hydrol. Earth Syst. Sci.*, *11*(5), 1633-1644. https://doi.org/10.5194/hess-11-1633-2007

Pina, R. D., Ochoa-Rodriguez, S., Simões, N. E., Mijic, A., Marques, A. S., & Maksimović, Č. (2016). Semi- vs. fully-distributed urban stormwater models: Model set up and comparison with two real case studies. *Water*, *8*(2), 58.

Qi, W., Ma, C., Xu, H., Chen, Z., Zhao, K., & Han, H. (2021). A review on applications of urban flood models in flood mitigation strategies. *Natural Hazards*, *108*(1), 31-62. https://doi.org/10.1007/s11069-021-04715-8

Rossman, L. A. (2015). *Storm water management model-User's manual version 5.1*. https://www.epa.gov/sites/default/files/2019-02/documents/epaswmm5_1_manual_master_8-2-15.pdf

Rossman, L. A., & Huber, W. C. (2016). *Storm water management model reference manual -Volume I – Hydrology*. https://nepis.epa.gov/Exe/ZyPDF.cgi?Dockey=P100NYRA.txt

Saghafian, B., Farazjoo, H., Bozorgy, B., & Yazdandoost, F. (2008). Flood intensification due to changes in land use. *Water Resources Management*, *22*(8), 1051-1067. https://doi.org/10.1007/s11269-007-9210-z

Salvadore, E., Bronders, J., & Batelaan, O. (2015). Hydrological modelling of urbanized catchments: A review and future directions. *Journal of Hydrology*, *529*, 62-81. https://doi.org/https://doi.org/10.1016/j.jhydrol.2015.06.028

Sanyal, J., Densmore, A., & Carbonneau, P. (2014). Analysing the effect of land-use/cover changes at sub-catchment levels on downstream flood peaks: A semi-distributed modelling approach with sparse data. *CATENA*, *118*, 28–40. https://doi.org/10.1016/j.catena.2014.01.015

Sanz-Ramos, M., Bladé, E., González-Escalona, F., Olivares, G., & Aragón-Hernández, J. L. (2021). Interpreting the Manning roughness coefficient in overland flow simulations with coupled hydrological-hydraulic distributed models. *Water*, *13*(23), 3433.

Sari, H. (2022). The effect of some soil characteristics on the hydraulic conductivity of soil in tekirdağ province [Research Articles]. *32*. https://doi.org/https://dergipark.org.tr/en/pub/alinterizbd/issue/33578/347179

Schirmer, M., Leschik, S., & Musolff, A. (2012). Current research in urban hydrogeology – A review. *advances in water resources*, *51*, 280-291. https://doi.org/10.1016/j.advwatres.2012.06.015

Serre, D., & Heinzlef, C. (2018). Assessing and mapping urban resilience to floods with respect to cascading effects through critical infrastructure networks. *International Journal of Disaster Risk Reduction*, *30*, 235-243. https://doi.org/https://doi.org/10.1016/j.ijdrr.2018.02.018

Shuster, W. D., Bonta, J., Thurston, H., Warnemuende, E., & Smith, D. R. (2005). Impacts of impervious surface on watershed hydrology: A review. *Urban Water Journal*, *2*(4), 263-275. https://doi.org/10.1080/15730620500386529

Singh, A., Dawson, D., Trigg, M., & Wright, N. (2021). A review of modelling methodologies for flood source area (FSA) identification. *Natural Hazards*, *107*(2), 1047-1068. https://doi.org/10.1007/s11069-021-04672-2

State Water Resources Control Board. (2009). *Runoff coefficient (C) fact sheet*. Retrieved April 20 from https://www.waterboards.ca.gov/water_issues/programs/swamp/docs/cwt/guidance/513.pdf

Storteig, I. (2019). *Continuous urban hydrological modeling of discharge peaks with SWMM [Master's thesis].* University of Oslo.

Sæten, R. B. (2021). *Pore pressure evolution and related risk at Gaustad [Master's thesis].* University of Oslo].

Teng, J., Jakeman, A. J., Vaze, J., Croke, B. F. W., Dutta, D., & Kim, S. (2017). Flood inundation modelling: A review of methods, recent advances and uncertainty analysis. *Environmental Modelling & Software*, *90*, 201-216. https://doi.org/https://doi.org/10.1016/j.envsoft.2017.01.006

The Norwegian Centre for Climate Services (NCCS). (2017). *Climate in Norway 2100 – a knowledge base for climate adaptation*. https://www.miljodirektoratet.no/publikasjoner/2017/mai-2017/climate-in-norway-2100--a-knowledge-base-for-climate-adaptation/

Velpuri, N. M., Senay, G. B., Singh, R. K., Bohms, S., & Verdin, J. P. (2013). A comprehensive evaluation of two MODIS evapotranspiration products over the conterminous United States: Using point and gridded FLUXNET and water balance ET. *Remote Sensing of Environment*, *139*, 35-49. https://doi.org/https://doi.org/10.1016/j.rse.2013.07.013

Welty, C. (2009). The Urban Water Budget.

Wihlborg, M., Sörensen, J., & Alkan Olsson, J. (2019). Assessment of barriers and drivers for implementation of blue-green solutions in Swedish municipalities. *Journal of Environmental Management*, *233*, 706-718. https://doi.org/https://doi.org/10.1016/j.jenvman.2018.12.018

Wilby, R. L., & Keenan, R. (2012). Adapting to flood risk under climate change. *Progress in Physical Geography: Earth and Environment*, *36*(3), 348-378. https://doi.org/10.1177/0309133312438908

Xichao, G., Yang, Z., Han, D., Huang, G., & Zhu, Q. (2020). *A Framework for Automatic Calibration of SWMM Considering Input Uncertainty*. https://doi.org/10.5194/hess-2020-367

Ye, A., Zhou, Z., You, J., Ma, F., & Duan, Q. (2018). Dynamic Manning's roughness coefficients for hydrological modelling in basins. *Hydrology Research*, *49*(5), 1379-1395. https://doi.org/10.2166/nh.2018.175

Zahmatkesh, Z., Burian, S. J., Karamouz, M., Tavakol-Davani, H., & Goharian, E. (2015). Low-Impact Development practices to mitigate climate change effects on urban stormwater runoff: Case study of New York City. *Journal of Irrigation and Drainage Engineering*, *141*(1), 04014043. https://doi.org/doi:10.1061/(ASCE)IR.1943-4774.0000770

Zhang, D., Gersberg, R. M., Ng, W. J., & Tan, S. K. (2017). Conventional and decentralized urban stormwater management: A comparison through case studies of Singapore and Berlin, Germany. *Urban Water Journal*, *14*(2), 113-124. https://doi.org/10.1080/1573062X.2015.1076488

Appendix

Table A.1: Average values of Manning's n for subcatchments based on subcatchment land cover

Subcatchment ID	Pervious area* (m2)	Gravel road (m2)	n gravel road	Garden (m2)	n garden	Natural area (m2)	n natural area	n pervious
1	10362.31	1786	0.02	8576.31	0.17	-	0.13	0.14
2	3605.41	440	0.02	3165.41	0.17	-	0.13	0.15
3	1044.8	44	0.02	1000.8	0.17	-	0.13	0.16
4	8843.88	888	0.02	7955.88	0.17	-	0.13	0.15
5	3918.14	-	0.02	3918.14	0.17	-	0.13	0.15
6	1607.36	222	0.02	1385.36	0.17	-	0.13	0.15
8	19743.72	-	0.02	19743.72	0.17	19743	0.13	0.13
9	8814.49	1820	0.02	6994.49	0.17	-	0.13	0.14
10	1120.84	-	0.02	1120.84	0.17	-	0.13	0.13
12	5278.79	-	0.02	5278.79	0.17	5278.79	0.13	0.15
13	9267.72	690	0.02	8577.72	0.17	-	0.13	0.16
14	4094.56	549	0.02	3545.56	0.17	-	0.13	0.15
15	11909.06	1008	0.02	10901.06	0.17	-	0.13	0.16
16	138.89	-	0.02	138.89	0.17	138.89	0.13	0.13
17	1358.41	29	0.02	1329.41	0.17	-	0.13	0.17
18	122.94	-	0.02	122.94	0.17	122.94	0.13	0.13
19	1257.49	56	0.02	1201.49	0.17	-	0.13	0.16
20	2808.97	-	0.02	2808.97	0.17	2808.97	0.13	0.13
21	1729.34	-	0.02	1729.34	0.17	-	0.13	0.17
22	155.57	-	0.02	155.57	0.17	-	0.13	0.17
24	9103.29	724	0.02	8379.29	0.17	-	0.13	0.16
25	11489.2	1278	0.02	10211.2	0.17	-	0.13	0.15

*Pervious area includes gravel road, garden, and natural area

Table A.2: Average values of Manning's n for each conduit (open channel) specified for the left, middle, and right of the channel based on land covers

Conduit ID	Transect ID	Left bank				Main channel				Right bank			
		Building area %	Asphalt/concrete area %	natural area %	n overall	Building area %	Asphalt/concrete area %	natural area %	n overall	Building area %	Asphalt/concrete area%	natural area%	n overall
Con10	1	12.56	0.00	87.44	0.048	0.00	0.00	10.00	0.040	0.00	0.00	10.00	0.040
Con11	2	0.00	0.00	10.00	0.040	0.00	0.00	10.00	0.040	0.00	0.00	10.00	0.040
con12	3	20.22	0.00	79.78	0.052	17.27	0.00	82.73	0.050	0.00	0.00	10.00	0.040
con13	4	6.30	0.00	93.70	0.044	0.00	0.00	10.00	0.040	0.00	0.00	10.00	0.040
Con14	5	0.00	0.00	10.00	0.040	0.00	0.00	10.00	0.040	0.00	0.00	10.00	0.040
Con20	6	11.38	0.00	88.62	0.047	0.00	10.81	89.19	0.037	0.00	0.00	10.00	0.040
Con21	7	5.18	0.00	94.82	0.043	0.00	16.88	83.12	0.036	0.00	0.00	10.00	0.040
Con22	8	4.20	0.00	95.80	0.043	0.00	8.63	91.37	0.038	0.00	0.00	10.00	0.040
Con30	9	2.03	0.00	97.97	0.041	0.00	28.30	71.70	0.033	0.00	0.00	10.00	0.040
Con40	10	11.80	0.00	88.20	0.047	0.00	30.67	69.33	0.032	0.00	0.00	10.00	0.040
Con50	11	0.00	0.00	10.00	0.040	0.00	15.89	84.11	0.036	0.00	0.00	10.00	0.040
CSU	44	0.00	0.00	10.00	0.040	0.00	32.69	67.31	0.032	0.00	0.00	10.00	0.040
Con60	42	0.00	0.00	10.00	0.040	0.00	0.00	10.00	0.040	0.00	0.00	10.00	0.040
Con65	37	0.00	15.63	84.38	0.036	0.00	65.57	34.43	0.024	0.00	36.96	63.04	0.031
Con66	36	0.00	23.61	76.39	0.034	0.00	12.11	87.89	0.037	0.00	0.00	10.00	0.040
Con67	35	26.18	0.00	73.82	0.056	1.44	20.00	78.56	0.036	12.04	0.00	87.96	0.047
Con68	34	0.00	0.00	0.00	0.040	0.00	22.30	77.70	0.034	0.00	0.00	10.00	0.040
Con69	33	10.00	0.00	0.00	0.010	0.00	17.01	82.99	0.036	0.00	0.00	10.00	0.040
Con70	32	0.00	12.92	87.08	0.037	0.00	19.20	80.80	0.035	0.00	0.00	10.00	0.040
Con71	31	27.97	14.69	57.34	0.053	0.00	21.32	78.68	0.035	0.00	0.00	10.00	0.040
Con80	30	49.69	11.32	38.99	0.067	0.00	24.51	75.49	0.034	0.00	0.00	10.00	0.040
Con81	29	51.55	13.21	35.23	0.068	0.00	28.57	71.43	0.033	0.00	0.00	10.00	0.040
Con82	28	40.22	13.33	46.45	0.061	0.00	21.79	78.21	0.035	0.00	0.00	10.00	0.040
Con10	1	12.56	0.00	87.44	0.048	0.00	0.00	10.00	0.040	0.00	0.00	10.00	0.040
Con11	2	0.00	0.00	10.00	0.040	0.00	0.00	10.00	0.040	0.00	0.00	10.00	0.040
con12	3	20.22	0.00	79.78	0.052	17.27	0.00	82.73	0.050	0.00	0.00	10.00	0.040
con13	4	6.30	0.00	93.70	0.044	0.00	0.00	10.00	0.040	0.00	0.00	10.00	0.040
Con14	5	0.00	0.00	10.00	0.040	0.00	0.00	10.00	0.040	0.00	0.00	10.00	0.040
Con20	6	11.38	0.00	88.62	0.047	0.00	10.81	89.19	0.037	0.00	0.00	10.00	0.040
Con21	7	5.18	0.00	94.82	0.043	0.00	16.88	83.12	0.036	0.00	0.00	10.00	0.040
Con22	8	4.20	0.00	95.80	0.043	0.00	8.63	91.37	0.038	0.00	0.00	10.00	0.040
Con30	9	2.03	0.00	97.97	0.041	0.00	28.30	71.70	0.033	0.00	0.00	10.00	0.040

Table A.3 Manually calculated runoff coefficients and runoff coefficients from the SWMM model and the variation for the subcatchments

Subcatchment ID	Manually calculated runoff coefficient	Runoff coefficient from SWMM model	Variation
S 1	0.25	0.261	1
S 2	0.25	0.27	2
S 3	0.25	0.302	5
S 4	0.30	0.291	-1
S 5	0.50	0.59	9
S 6	0.30	0.319	2
S 8	0.40	0.43	3
S 9	0.30	0.269	-3
S 10	0.40	0.434	3
S 12	0.20	0.252	5
S 13	0.30	0.289	-1
S 14	0.30	0.31	1
S 15	0.35	0.335	-2
S 16	0.35	0.403	5
S 17	0.25	0.296	5
S 18	0.35	0.424	7
S 19	0.30	0.345	5
S 20	0.40	0.417	2
S 21	0.30	0.334	3
S 22	0.55	0.645	10
S 24	0.30	0.308	1
S 25	0.30	0.282	-2

A.4.Average and maximum water depth in nodes

Node ID	Type	Average water depth (m)	Day of simulation	Time (hr:min)	Maximum water depth (m)
J010	JUNCTION	0	220	16:11	0.07
J011	JUNCTION	0	220	16:12	0.07
J012	JUNCTION	0	220	16:12	0.09
J013	JUNCTION	0	220	16:13	0.09
J014	JUNCTION	0	220	16:13	0.11
J020	JUNCTION	0	220	16:14	0.11
J021	JUNCTION	0	944	23:43	0.1
J022	JUNCTION	0	944	23:43	0.1
J030	JUNCTION	0	944	23:43	0.24
J040	JUNCTION	0	944	23:44	0.24
J050	JUNCTION	0	944	23:44	0.09
J060	JUNCTION	0	944	23:41	0.19
J065	JUNCTION	0	944	23:45	0.19
J066	JUNCTION	0	944	23:46	0.07
J067	JUNCTION	0	944	23:46	0.07
J068	JUNCTION	0	944	23:47	0.07
J069	JUNCTION	0	944	23:48	0.09
J070	JUNCTION	0	944	23:46	0.11
J071	JUNCTION	0	944	23:46	0.18
J080	JUNCTION	0	944	23:46	0.18
J081	JUNCTION	0	944	23:46	0.13
J082	JUNCTION	0	944	23:46	0.13
J090	JUNCTION	0	944	23:41	0.02
OF01	OUTFALL	0	944	23:42	0.02
SU01	STORAGE	0.1	220	18:17	1.94

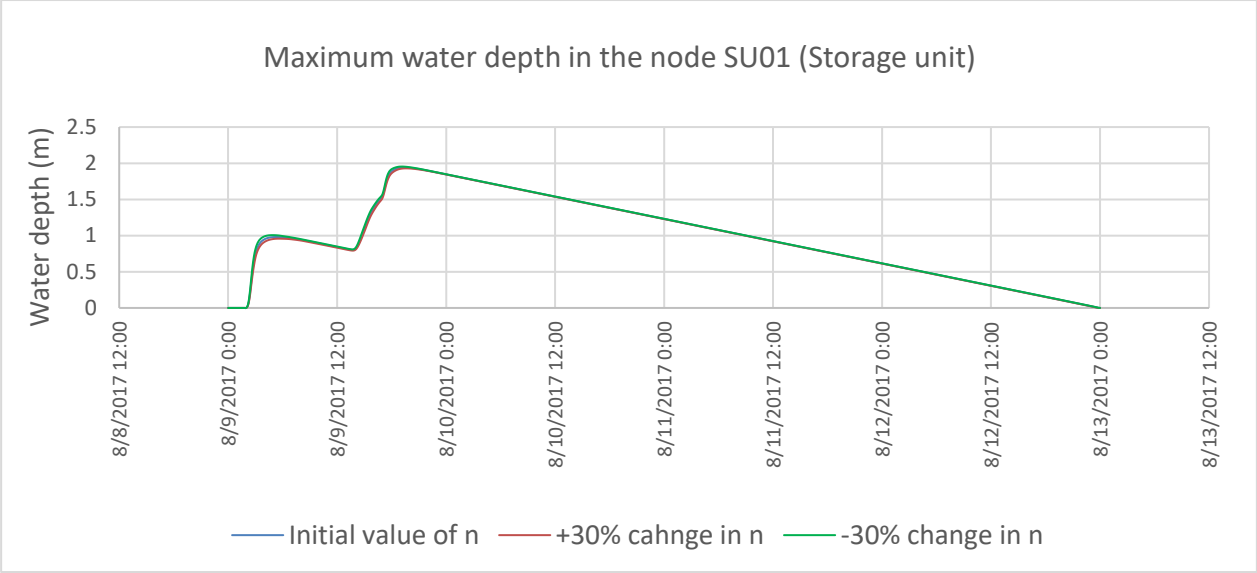

Figure A-1: Water depth in the node SU01 associated with the peak discharge of 0.983 m3/s on 9.8.2017 for ±30 change in the initial value of Manning's n for subcatchments

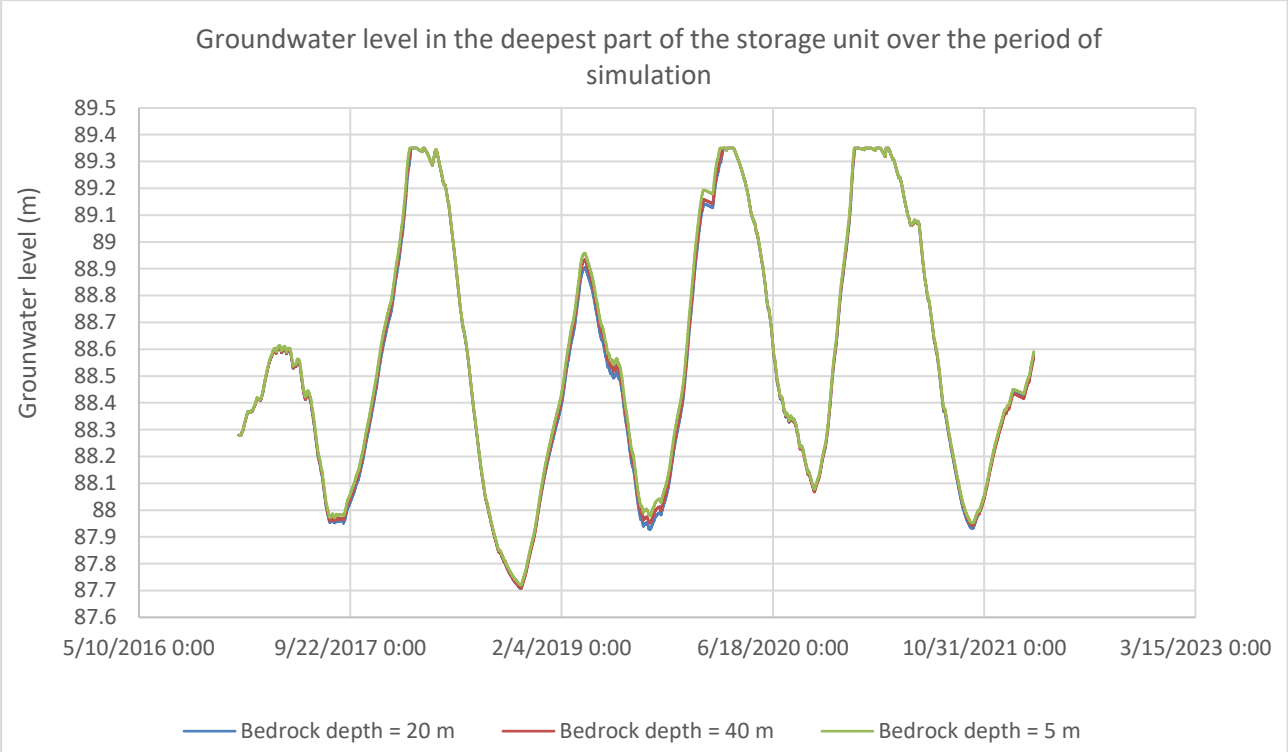

Figure A-2: The effects of different scenarios of bedrock depth on groundwater level in subcatchment 17(associated with the deepest part of the storage unit)